CAPITAL UNIVERSITY OF SCIENCE AND
TECHNOLOGY, ISLAMABAD

Scattering of Acoustic Wave from a Rectangular Membrane in 3D Waveguide

by

Azhar Mahmood

A thesis submitted in partial fulfillment for the
degree of Master of Philosophy

in the

Faculty of Computing
Department of Mathematics

2025

I dedicate this effort to my Family, my dear Parents, my elegant Teachers and my supervisor Dr. Muhammad Afzal who are always source of inspiration for me and their contributions are uncounted.

CERTIFICATE OF APPROVAL

Scattering of Acoustic Wave from a Rectangular Membrane in 3D Waveguide

by

Azhar Mahmood

(MMT223001)

THESIS EXAMINING COMMITTEE

S. No.	Examiner	Name	Organization
(a)	External Examiner	Dr. Tufail Ahmed Khan	UET, Peshawar
(b)	Internal Examiner	Dr. Abdul Rehman Kashif	CUST, Islamabad
(c)	Supervisor	Dr. Muhammad Afzal	CUST, Islamabad

Dr. Muhammad Afzal
Thesis Supervisor
April 2025

Dr. Muhammad Sagheer
Head
Dept. of Mathematics
April, 2025

Dr. Muhammad Abdul Qadir
Dean
Faculty of Computing
April, 2025

Author's Declaration

I, **Azhar Mahmood**, hereby state that my MPhil thesis titled "**Scattering of Acoustic Wave from a Rectangular Membrane in 3D Waveguide** " is my work and has not been submitted previously by me for taking any degree from Capital University of Science and Technology, Islamabad or anywhere else in the country/abroad.

At any time if my statement is found to be incorrect even after my graduation, the University has the right to withdraw my MPhil Degree.

(Azhar Mahmood)

Registration No: MMT223001

Plagiarism Undertaking

I solemnly declare that the research work presented in this thesis titled "**Scattering of Acoustic Wave from a Rectangular Membrane in 3D Waveguide**" is solely my research work with no significant contribution from any other person. Small contribution/help wherever taken has been dully acknowledged and that complete thesis has been written by me.

I understand the zero tolerance policy of the HEC and Capital University of Science and Technology towards plagiarism. Therefore, I as an author of the above-titled thesis declare that no portion of my thesis has been plagiarized and any material used as reference is properly referred/cited.

I undertake that if I am found guilty of any formal plagiarism in the above-titled thesis even after awarded of MPhil Degree, the University reserves the right to withdraw/revoke my MPhil degree and that HEC and the University have the right to publish my name on the HEC/University website on which names of students are placed who submitted plagiarized work.

(Azhar Mahmood)

Registration No: MMT223001

Acknowledgement

I got no words to articulate my cordial sense of gratitude to **Almighty Allah** who is the most merciful and most beneficent to his creation.

I also express my gratitude to the last prophet of **Almighty Allah, Prophet Muhammad (PBUH)** the supreme reformer of the world and knowledge for a human being.

I would like to be thankful to all those who provided support and encouraged me during this work.

I would like to be grateful to my thesis supervisor **Dr. Muhammad Afzal,** for guiding and encouraging me in writing this thesis. It would have remained incomplete without his endeavours. Due to his efforts, I was able to write and complete this assertation.

I would like to pay great tribute to my **parents**, for their prayers, moral support, encouragement and appreciation.

Last but not the least, I want to express my gratitude to my **friends** who helped me throughout my MPhil degree.

(Azhar Mahmood)

Abstract

This research focuses on the modeling and analysis of Acoustic wave scattering from a rectangular membrane situated within a three-dimensional waveguide. The first problem contains a membrane situated within an infinite three-dimensional waveguide. The second problem contains a membrane backed by a rigid cavity, and the third problem contains a membrane backed by soft wall. The membrane is positioned inside rectangular waveguide and is connected to the surface through spring-like boundary conditions. The mathematical framework governing wave propagation involves a system of differential equations, including the Helmholtz's equation, the membrane equation and rigid boundary conditions. To solve the resulting boundary value problems, the Mode-Matching technique is employed. Eigenfunction expansion with unknown amplitudes is discovered in duct regions, and matching conditions at the interfaces helps in converting the differential system into a linear algebraic system, which is then truncated and solved. The truncated solution satisfies the matching conditions.

Contents

List of Figures

Abbreviations

BEM	Boundary element method
BVPs	Boundary value problems
CFD	Computational fluid dynamics
CMPP	Compound micro-perforated panel
FEM	Finite element method
HVAC	Heating, Ventilation, and Air Conditioning
MM	Mode-Matching
MPM	Micro-perforated membrane
MPP	Micro-perforated panel

Symbols

c	Speed of sound
ρ	Fluid density
P	Acoustic pressure
k	Wave number
U	Membrane displacement
V	Velocity vector
T	Tension
ρ_m	Mass density
c_m	Speed of wave on membrane
ϕ	Fluid potential
t	Harmonic time dependence
μ	Membrane wave number
α	Fluid loading parameter
ψ_{mn}	Eigenfuntion
∇	Divergence
η_{mn}	Mode wave number
A_{mn}	Amplitude of propagating modes
g	Gravitational acceleration
$\bigtriangledown p$	Exerting force
ρg	Body force
δ_{mn}	Kronecker delta

Chapter 1

Introduction

When a flexible material is capable of vibration, it can significantly impact the scattering of waves, such as sound waves, light waves, or other types of vibrations. The flexibility of the material allows it to deform and change shape in response to the vibration, which can alter the way that waves interact with the material.

One of the key effects of flexible materials on scattering is the creation of a dynamic scattering pattern. As the material vibrates, its surface can oscillate and create a time-dependent scattering pattern.

This can lead to a number of interesting effects, including the modification of the scattering cross-section, the creation of new scattering modes, and the enhancement of certain scattering phenomena. For example, in the case of sound waves, a flexible material can create a dynamic scattering pattern that can affect the way that sound waves are absorbed, transmitted, or reflected by the material.

This can be particularly important in applications such as soundproofing, where the goal is to minimize the transmission of sound waves through a material. In addition to the dynamic scattering pattern, the flexibility of the material can also introduce additional degrees of freedom that can scatter waves in unique and complex ways. For example, a flexible material can bend or twist in response to a vibration, which can create new scattering modes that are not present in rigid materials.

The impact of flexible materials on scattering can also be influenced by the properties of the material itself, such as its density, elasticity, and damping characteristics. For example, a material with high damping characteristics can absorb more energy from the vibration, which can reduce the amount of scattering that occurs. In general, the interaction between flexible materials and vibration can lead to rich and complex scattering behavior, with many potential applications in fields such as materials science, physics, and engineering. Some of the potential applications of flexible materials in scattering include soundproofing, vibration isolation, and the design of novel materials with unique scattering properties.

In terms of specific examples, flexible materials can be used to create novel scattering systems, such as metamaterials, which can exhibit unique properties such as negative refractive index or perfect absorption. Flexible materials can also be used to create tunable scattering systems, where the scattering properties can be adjusted in real-time by changing the vibration frequency or amplitude. Furthermore, flexible materials can also be used to create scattering systems that can operate in a wide range of frequencies, from low-frequency sound waves to high-frequency light waves. This can be particularly important in applications such as sensing, where the goal is to detect and analyze waves over a wide range of frequencies.

In conclusion, the impact of flexible materials on scattering is a complex and multifaceted topic, with many potential applications in fields such as materials science, physics, and engineering. By understanding the ways in which flexible materials can interact with vibrations and scatter waves, researchers and engineers can design novel materials and systems with unique properties and capabilities.

1.1 Literature review

Acoustic membranes are thin, flexible materials that are designed to transmit or manipulate sound waves. They are commonly used in a variety of applications, including soundproofing, noise reduction, and acoustic treatment. Some of the key characteristics of acoustic membranes include that acoustic membranes can provide high levels of sound insulation, with sound transmission losses of up to 30-40 dB. Low-frequency

response: These membranes can be designed to respond to low frequencies, making them effective in controlling rumble and bass sounds. Acoustic membranes can be designed to be highly transparent, allowing minimal visual impact and preserving the aesthetic appeal of a space. These membranes can be made from a variety of materials, including metals, plastics, and fabrics, and can be designed to be flexible and conform to complex shapes. Overall, acoustic membranes play a crucial role in many applications where sound waves need to be transmitted, manipulated, or controlled. Cao and Wang [1] presented a study on the optimization of acoustic membrane panels for sound absorption. Wang et al. [2] introduced the manufacturing of membrane acoustical metamaterials for low frequency noise reduction and control. Naify et al. [3] discussed the transmission loss and dynamic response of locally resonant membrane-type acoustic materials. Boccaccio et al. [4] used a multifunctional ultrathin acoustic membrane with self-healing properties for adaptive low-frequency noise control. Maa's work [5] introduced the concept of microperforated panels for sound absorption, including the design and optimization of microperforated panels for acoustic applications. An acoustic microperforated membrane is a type of membrane that has a large number of small holes or perforations, typically with diameters in the range of 0.1-1.0 mm. These perforations are designed to allow sound waves to pass through the membrane while maintaining a high level of sound insulation. The concept of acoustic microperforated membranes was first introduced in the 1980s, and since then, they have been widely used in various applications, including soundproofing, noise reduction, and acoustic treatment. Gai et al. [6] proposed a hybrid sound-absorbing structure that integrates a micro-perforated plate with a Helmholtz composite, which enables effective sound absorption at lower frequencies, a range where traditional sound-absorbing materials often struggle to perform well.

Li et al. [7] developed a new theoretical model for calculating the acoustic impedance of micro-perforated membranes, which takes into account the velocity continuity condition at the perforation boundary. Lee et al. [8] presented a theoretical and numerical study on the sound absorption of a finite flexible micro-perforated panel backed by an air cavity. Guo and Min [9] presented a study on a novel sound absorber design that utilizes a compound micro-perforated panel (CMPP) with partitioned cavities of different depths. Kang and Fuchs [10] presented a theoretical model for predicting the

sound absorption of open weave textiles and microperforated membranes backed by an air space. The unique properties of these membranes make them an attractive solution for controlling sound waves in a wide range of frequencies. The working principle of an acoustic microperforated membrane is based on the idea that the small perforations create a high-impedance surface that reflects sound waves, while the membrane itself provides a low-impedance path for sound waves to pass through. This combination of high- and low-impedance surfaces creates a resonant cavity that can be tuned to specific frequencies, allowing for effective sound insulation and noise reduction.

Acoustic microperforated membranes can provide high levels of sound insulation, with noise transmission losses of up to 30-40 dB. These membranes can be designed to respond to low frequencies, making them effective in controlling rumble and bass sounds. Acoustic microperforated membranes can be designed to be highly transparent, allowing for minimal visual impact and preserving the aesthetic appeal of a space. These membranes can be made from a variety of materials, including metals, plastics, and fabrics, and can be designed to be flexible and conform to complex shapes.

Overall, acoustic microperforated membranes are a powerful tool for controlling sound waves and improving acoustic performance in a wide range of applications. Their unique combination of high sound insulation, low frequency response, and high transparency make them an attractive solution for soundproofing, noise reduction, and acoustic treatment.

The restrain edge on a membrane refers to the boundary or edge of the membrane that is fixed or restrained in some way, preventing it from moving or vibrating freely. In other words, the restrain edge is the edge of the membrane that is clamped, fixed, or attached to a rigid structure, such as a frame or a support, which restricts its motion. The restraint edge can have a significant impact on the behavior and performance of the membrane, particularly in terms of its vibration and sound transmission characteristics. For example, the limit edge can affect the boundary conditions of the membrane, which in turn can influence the natural frequencies, modes, and loss of sound transmission. Liu and Chen's [11] research investigated the effect of restrain edge on sound transmission loss of membrane panels, including the impact of edge restraint on sound wave propagation and transmission. Wang et al. [12] examined

the influence of restrain edge on acoustic performance of microperforated membrane panels, including the effects of edge restraint on sound absorption and sound transmission. Liu and Chen [13] presented an experimental investigation on the effect of edge restraint on the sound radiation of membrane panels made of different materials. The restraint edge can help suppress vibrations and reduce the transmission of sound waves through the membrane, particularly at high frequencies. The restraint edge can also create stress concentrations in the membrane, particularly at the points where the membrane is attached to the rigid structure. This can lead to increased stress and potential failure of the membrane. The choice of a restrain edge will depend on the specific application and requirements of the membrane, as well as the desired performance characteristics. For example, in soundproofing applications, a clamped edge may be used to maximize sound transmission loss, while in vibration isolation applications, a simply supported or free edge may be used to allow for greater flexibility and vibration suppression. Earlier studies often idealized plate boundaries using perfectly clamped conditions. However, such idealization rarely holds in real-world applications, where boundaries typically exhibit elastic or partially constrained behavior, as demonstrated in several recent investigations [14–26].

A variety of methodological approaches exist for the analysis and solution of problems involving acoustic membranes and microperforated membranes. These methods can be broadly classified into numerical, analytical, and experimental techniques, each offering distinct advantages depending on the complexity of the problem, the geometry of the system, and the desired level of accuracy. Among numerical approaches, the Finite Element Method (FEM) is one of the most widely adopted. FEM discretizes the structure into a mesh of finite elements, allowing the governing equations of motion to be solved at the element level. This method is particularly advantageous for dealing with complex geometries, inhomogeneous materials, and varying boundary conditions, making it ideal for detailed simulations of acoustic behavior in membrane systems. The Boundary Element Method (BEM) serves as another powerful numerical tool, distinguished by its focus on boundary conditions rather than the entire domain. By reducing the dimensionality of the problem, BEM offers computational efficiency, particularly in scenarios involving unbounded domains—a common occurrence in acoustic radiation and scattering problems.

Analytical methods provide a complementary perspective by enabling exact or approximate solutions to the governing equations through mathematical formulations. Techniques such as separation of variables, Fourier transforms, and eigenfunction expansions are frequently employed. Although typically limited to simpler geometries and ideal boundary conditions, analytical approaches offer valuable theoretical insights and serve as benchmarks for validating numerical simulations. Experimental techniques are equally essential in advancing the understanding of acoustic and microperforated membranes. Through physical measurements in controlled environments, experimental methods allow for the validation of computational models and provide empirical insights into phenomena that may be challenging to predict analytically or numerically. These studies often inform the development of practical noise control solutions and guide the refinement of theoretical models.

The mode matching technique is an analytical method widely used to solve wave propagation and scattering problems in various domains, including acoustics, electromagnetics, and optics. It involves representing the wave field as a superposition of modes—solutions to the wave equation that satisfy the boundary conditions of the problem. These modes are typically orthogonal, enabling efficient and accurate representation of the wave behavior within complex systems. Despite its computational intensity, the mode matching technique remains a fundamental and dependable tool for researchers and engineers. Its versatility and accuracy make it especially valuable in addressing problems involving complex boundary and interface conditions [27–38].

Mode matching has gained significant traction in acoustic applications, particularly for the modeling of membrane-based structures aimed at noise reduction. It has proven highly effective in handling systems with geometric discontinuities, layered configurations, and flexible boundaries, allowing for precise prediction of wave transmission, reflection, and attenuation. Its utility in these applications is demonstrated in a growing body of recent research [39–49].

Historically, the mode matching technique was introduced by Mittra [50] to analyze guided wave phenomena in waveguides and antennas. Building on this foundation, Kok and Mittra [51] extended the technique to solve broader electromagnetic problems. Waterman [52] contributed a matrix-based formulation of mode matching to

address complex scattering problems, laying further groundwork for its application in various scientific disciplines. In acoustics, Chen and Wang [53] developed a numerical mode matching approach capable of handling wave propagation in geometrically intricate domains, emphasizing its practicality for real-world scenarios.

More recently, Deng et al. [54] examined the use of acoustic metamaterials particularly polymer-based variants for manipulating acoustic radiation. Their review highlighted various strategies for controlling wave behavior and the design principles behind such engineered materials, many of which rely on theoretical frameworks compatible with mode matching methods. Complementary to wave-based modeling approaches, several foundational studies have explored the mechanics of plate and membrane structures, which are often components in acoustic systems. Reissner [55] investigated the influence of transverse shear deformation on the bending behavior of elastic plates, offering a fundamental understanding critical for advanced structural modeling. Dow [56] introduced a bonded plate model to describe the vibration of thin plates, providing insight into the dynamic characteristics of layered structures. Similarly, Huang [57] developed a framework for analyzing rectangular plates with free edges, further enriching the analytical tools available for evaluating the performance of complex acoustic elements. Together, these developments have solidified the role of mode matching as a cornerstone in the analysis of wave propagation in both rigid and flexible media. Its integration with modern theories of plate and membrane mechanics has expanded its applicability, making it a crucial technique for advancing the design and analysis of innovative noise control solutions.

1.2 Thesis Structure

This thesis consists of five chapters.

- **Chapter 1** serves as an introduction to the research presented in this thesis, incorporating a detailed review of existing literature to provide essential context. It lays the groundwork for the study by exploring relevant theoretical frameworks and empirical findings that have influenced the research direction.

- **Chapter 2** provides some basic definitions, physical laws, and formulation of membrane equation.

- **Chapter 3** contains scattering of acoustic wave from a rectangular membrane in infinite 3D rectangular duct.

- **Chapter 4** contains scattering of acoustic wave from a rectangular membrane in 3D waveguide.

- **Chapter 5** provides the concluding remarks of the present study.

The references used in the thesis are mentioned in **Bibliography**.

Chapter 2

Preliminaries

This chapter provides foundational definitions and laws that will serve as a useful reference for the chapters that follow.

2.1 Acoustic

The field of acoustics has experienced significant growth since its beginnings, evolving from the initial study of audible sound waves to encompass a vast range of frequencies and applications. Covering areas such as structural, environmental, and bioacoustics, it integrates knowledge from multiple disciplines, including physics, engineering, and music.

2.2 Acoustic Wave Equation

The behavior of acoustic waves in a medium like air can be mathematically modeled using equations based on fundamental physical principles such as mass, momentum, and energy conservation. However, these equations are often complex and nonlinear, making analysis challenging. To address this, a linear approximation is typically employed, simplifying the equations and enabling a more straightforward examination of wave propagation, thereby providing valuable understanding of acoustic wave behavior in the medium.

2.2.1 Conservation of Mass

The conservation of mass equation expresses the relationship between the rate of change of mass density within a specified volume and the net mass flow into or out of that volume, over a unit time period. Mathematically,

$$\frac{\partial \rho}{\partial t} + \nabla.(\rho \mathbf{u}) = 0. \tag{2.1}$$

In this context, $\mathbf{u}$ denotes the flow velocity, while ρ represents the instantaneous mass density.

2.2.2 Conservation of Momentum

The conservation of momentum equation relates the net momentum flow rate to the forces applied to the system that is

$$\frac{\partial \rho \mathbf{u}}{\partial t} = -\nabla.(\rho \mathbf{u})\mathbf{u} - \nabla p + \rho g. \tag{2.2}$$

Here, p represents pressure, g denotes gravitational acceleration, ∇p signifies the exerted force, and ρg indicates the body force, as evident from equation (2.1),

$$\frac{\partial \rho \mathbf{u}}{\partial t} + \nabla.(\rho \mathbf{u})\mathbf{u} = -\nabla p + \rho g. \tag{2.3}$$

This implies that

$$\left(\frac{\partial \rho}{\partial t} + \nabla.(\rho \mathbf{u})\right)\mathbf{u} = \rho\left(\frac{\partial}{\partial t} + \mathbf{u}.\nabla\right)\mathbf{u} = -\nabla p + \rho g. \tag{2.4}$$

Applying the continuity condition, we can express

$$\rho \frac{D\mathbf{u}}{Dt} = -\nabla p + \rho g, \tag{2.5}$$

where $\frac{D}{Dt} = \frac{\partial}{\partial t} + \mathbf{u} \cdot \nabla$ represents the total time derivative, also known as the Stokes total derivative, which comprises two components: the first term $\frac{\partial}{\partial t}$ denotes the local time derivative, while the second term $\mathbf{u} \cdot \nabla$ represents the convective derivative.

2.3 Membrane

In acoustic waveguides, membranes, which can take the form of thin plates or diaphragms, respond to sound waves with vibrations, thereby affecting wave propagation. Membranes fulfill various functions, including:

- Dividing the waveguide into distinct sections
- Introducing obstacles or discontinuities
- Selectively enhancing or suppressing specific frequency ranges
- Creating filters or resonators

Membranes exert significant influence over wave behavior, scattering, and transmission within the waveguide.

We consider a small rectangular element of a membrane with dimensions Δx and Δy, and thickness h. The displacement of the membrane at a position (x, y) and time t is denoted by $u(x, y, t)$.

2.3.1 Newton's Second Law

The net force acting on the membrane element is equal to its mass multiplied by its acceleration

$$F = ma. \tag{2.6}$$

2.3.2 Tension Forces

The tension forces in the membrane, denoted by T (tension per unit length), generate curvature along the x and y directions. These curvatures are represented by the second derivatives $\frac{\partial^2 u}{\partial x^2}$ and $\frac{\partial^2 u}{\partial y^2}$.

2.3.3 Acceleration of the Element

The acceleration of the membrane element is

$$a = \frac{\partial^2 u}{\partial t^2}. \tag{2.7}$$

2.3.4 Mass of the Membrane Element

The mass of the small membrane element is given by

$$m = \rho h(\Delta x \Delta y), \tag{2.8}$$

where ρ is the mass per unit area, and h is the thickness.

2.3.5 Force Balance

The net force due to tension is proportional to the sum of the second spatial derivatives

$$T(\Delta x \Delta y)\left(\frac{\partial^2 u}{\partial x^2} + \frac{\partial^2 u}{\partial y^2}\right) = \rho h(\Delta x \Delta y)\frac{\partial^2 u}{\partial t^2}, \tag{2.9}$$

which on dividing by $\Delta x \Delta y$ in (2.9), leads to

$$T\left(\frac{\partial^2 u}{\partial x^2} + \frac{\partial^2 u}{\partial y^2}\right) = \rho h \frac{\partial^2 u}{\partial t^2}. \tag{2.10}$$

2.3.6 Wave Speed

The wave speed c is defined as

$$c^2 = \frac{T}{\rho h}. \tag{2.11}$$

By using (2.11) into (2.10), we obtain the membrane wave equation:

$$\frac{\partial^2 u}{\partial t^2} = c^2\left(\frac{\partial^2 u}{\partial x^2} + \frac{\partial^2 u}{\partial y^2}\right). \tag{2.12}$$

This is the fundamental equation governing the behavior of vibrating membranes under tension.

2.3.7 Micro-Perforated Membrane

A micro-perforated elastic membrane is a thin, flexible sheet featuring tiny holes, known as micro-perforations, which enable the passage of acoustic energy while maintaining the membrane's structural integrity. This innovative design allow the membrane to effectively absorb sound energy, making it a popular choice for various acoustic applications, including:

- Sound absorption panels
- Acoustic filters
- Silencers
- Soundproofing materials

The micro-perforations create a large surface area, facilitating enhanced sound energy dissipation, while the membrane's elastic properties enable it to withstand mechanical stress and maintain its shape.

2.4 Impedance Conditions

2.4.1 Soft Conditions

The soft boundary conditions are Drichlet's type boundary conditions. In these type of conditions, the pressure or displacement is considered as zero, i.e.

$$\psi(x, y) = 0.$$

2.4.2 Rigid Conditions

Neumann's type boundary conditions are actually rigid boundary conditions. In rigid conditions, normal velocity is considered as zero, i.e.

$$\frac{\partial \psi}{\partial x} = 0.$$

2.4.3 Edge Conditions

Edge conditions in a waveguide are the boundaries or constraints imposed on the wavefield at the edges, determining how the wave behaves, such as reflection, absorption, or transmission. Common edge conditions include hard wall, soft wall, periodic, absorbing, and impedance boundaries.

2.4.4 Spring-like Conditions

Spring-like conditions in a waveguide or acoustic system are boundaries that:

- Allow displacement in response to force (pressure)
- Return to their original position when the force is removed
- Do not dissipate energy (no damping)

2.4.5 Fixed Conditions

In a waveguide, a fixed condition, also known as a "fixed boundary" or "clamped boundary", is a boundary where:

- The displacement (movement) is zero
- The wavefield is not allowed to move or vibrate
- The boundary is rigid and immovable

2.4.6 Free Conditions

In a waveguide, a free condition, also known as a "free boundary" or "unbounded boundary", is a boundary where:

- The wavefield is allowed to move or vibrate freely
- There are no constraints on the displacement (movement)
- The boundary is not rigid or fixed

2.5 Basic Definitions

2.5.1 Waveguides

Waveguides are specifically designed structures that guide waves, including electromagnetic waves and sound waves, in a way that minimizes energy loss. This is achieved by confining the wave's expansion to one or two dimensions. The shape and design of a waveguide dictate its functionality, with acoustic waveguides functioning similarly to transmission lines, effectively facilitating the propagation of sound waves within them.

2.5.2 Amplitude

Amplitude refers to the maximum magnitude or intensity of a wave, oscillation, or signal. Across various contexts, amplitude describes the following aspects:

- Sound waves: The loudness or intensity of a sound.
- Light waves: The brightness, luminosity, or intensity of light.
- Electrical signals: The magnitude of voltage or current level of an electrical signal.

- Vibrations: The magnitude or intensity of oscillations or vibrations.
- Mathematical functions: The maximum value that a function attains.

In essence, amplitude represents the "size" or "strength" of a wave or signal, typically measured from its equilibrium or zero point to its peak value.

2.5.3 Time Period

The time taken by a vibrating object to complete one cycle of motion is referred to as the time period. This duration is also known as the period of oscillation and is commonly denoted by the symbol T, formulated as:

$$T = \frac{2\pi}{\omega}. \tag{2.13}$$

2.5.4 Frequency

Frequency is the number of oscillations or cycles of a wave, signal, or vibration per unit time, typically measured in hertz (Hz), where 1 Hz equals one cycle per second.

Frequency is a fundamental property of waves and signals, playing a crucial role in various fields, including:

- Sound: Pitch and tone
- Light: Color and spectrum
- Electrical engineering: AC circuits and signal processing
- Vibrations: Mechanical resonance and structural analysis
- Physics: Wave behavior and quantum mechanics

Frequency is often represented by the symbol "f" and is related to other wave properties, such as wavelength and amplitude, through the speed of the wave.

2.5.5 Tension in Sound Waves

Tension plays a crucial role in sound propagation, particularly in solids and stretched media like strings, membranes, and rods. Unlike transverse waves in a string, where tension directly controls wave speed, sound waves are typically longitudinal, meaning particle motion is parallel to wave direction.

2.5.6 Effect of Tension on Sound Waves

2.5.6.1 Stretched Strings (Musical Instruments)

In stringed instruments such as guitars, violins, and pianos, tension directly influences the wave speed along the string, which affects the pitch of the sound produced.

- Increasing the tension increases the wave speed, resulting in a higher pitch.
- Decreasing the tension slows down the wave speed, producing a lower pitch.

The fundamental frequency f of a vibrating string is given by the equation

$$f = \frac{1}{2L}\sqrt{\frac{T}{\mu}}, \tag{2.14}$$

where:

f = fundamental frequency (Hz),
L = length of the string (m),
T = tension in the string (N),
μ = linear mass density (kg/m).

2.5.6.2 Tension in Membranes and Drumheads

In instruments like drums, the tension of the membrane affects its vibration and the resulting sound:

- Higher tension produces higher-pitched sounds due to increased wave speed.
- Lower tension creates deeper sounds by reducing the vibration frequency.
- Tension in solid rods and wires.

For solid materials, such as metal rods or taut wires, tension can influence the speed of longitudinal waves. The wave speed in a stretched wire is determined by

$$v = \sqrt{\frac{T}{\rho A}}, \tag{2.15}$$

where:

v = wave speed (m/s),
T = tension force (N),
ρ = material density (kg/m^3),
A = cross-sectional area (m^2).

2.6 Mode-Matching Scheme

Analytical approaches have been developed to study wave reflection, transmission, and absorption in waveguides. The choice of approach depends on the material and geometrical properties of the guiding structures and the underlying physical principles. Among these methods, the Mode-Matching (MM) technique is widely used for problems involving structural discontinuities and non-uniform impedance distributions.

The MM technique is a analytical method that solves acoustic problems by dividing the guiding structure into segments and determining the field potentials within each segment. The potentials are expanded in terms of unknown amplitudes, which are then determined by matching pressures and velocities at the interfaces between segments. This approach converts the differential system into a linear algebraic system, which is then solved for the unknown amplitudes. The MM technique has a broad range of applications in solving physical problems, including those in the automobile and HVAC industries, as well as various engineering structures. Its versatility and accuracy

make it a valuable tool in these fields. In the HVAC and automobile industries, duct-like structures play a crucial role in transferring vibrational energy, which can sometimes manifest as noise. Designing these elements to minimize noise is essential, often involving geometric modifications and material properties. The MM technique offers a relatively straightforward approach to finding solutions to these problems, providing an attractive method for tackling these challenges.

Chapter 3

Scattering of Acoustic Wave from a Rectangular Membrane in Infinite 3D Rectangular Duct

In this chapter, a rectangular membrane having area "ab" is contained in waveguide and scattering is discussed. The incident radiation are assumed to be the fundamental or higher order mode of rigid duct which passes after interaction with the membrane. This chapter is arranged such that Section 3.1 contains the mathematical formulation of the boundary value problem (BVP). The Mode-Matching solution is discussed in Section 3.2. The dynamics of membrane at interface is given in Section 3.3. The numerical results and discussion are given in Section 3.4.

3.1 Problem Formulation

Consider a rectangular waveguide having membrane at $\bar{z} = 0$, as shown in Fig. 3.1. The inside of waveguide is filled with compressible fluid of density ρ and sound speed c. The fluid potential in waveguide satisfies the dimensional wave equation

$$\bar{\nabla}^2\bar{\Phi}(\bar{x},\bar{y},\bar{z},\bar{t}) = \frac{1}{c^2}\frac{\partial^2\bar{\Phi}}{\partial\bar{t}^2}, \tag{3.1}$$

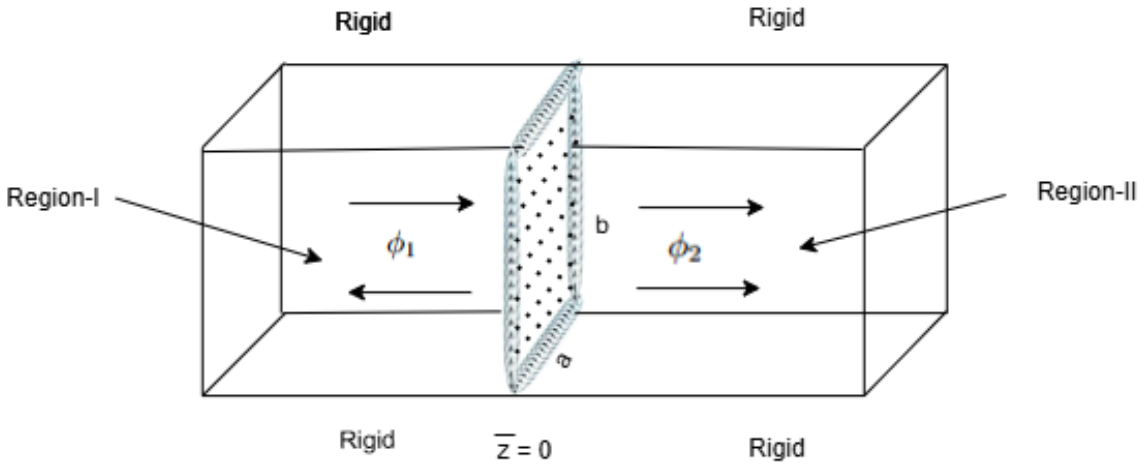

FIGURE 3.1: The physical configuration of waveguide

where overbars with variables show the dimensional setting of coordinates. The fluid potential $\bar{\Phi}$ is related to acoustic pressure $\bar{P}$ and velocity vector $\bar{V}$ through the relation

$$\bar{P} = -\rho \frac{\partial \bar{\Phi}}{\partial \bar{t}}, \tag{3.2}$$

and

$$\bar{V} = \bar{\nabla}\bar{\Phi}, \tag{3.3}$$

respectively. The boundary wall of waveguide is assumed acoustically rigid. The boundary conditions for acoustically rigid surface are:

$$\frac{\partial \bar{\Phi}}{\partial \bar{x}} = 0, \qquad \bar{x} = 0, \qquad \bar{x} = \bar{a}, \qquad 0 \leq \bar{y} \leq \bar{b}, \tag{3.4}$$

$$\frac{\partial \bar{\Phi}}{\partial \bar{y}} = 0, \qquad \bar{y} = 0, \qquad \bar{y} = \bar{b}, \qquad 0 \leq \bar{x} \leq \bar{a}. \tag{3.5}$$

At $\bar{z} = 0$, there exists a membrane. The membrane displacement $\bar{U}(\bar{x}, \bar{y}, \bar{z}, \bar{t})$ satisfies the equation

$$\frac{\partial^2 \bar{U}}{\partial \bar{x}^2} + \frac{\partial^2 \bar{U}}{\partial \bar{y}^2} - \frac{1}{c_m^2} \frac{\partial^2 \bar{U}}{\partial \bar{t}^2} = \frac{1}{T}(\bar{P}^+ - \bar{P}^-), \tag{3.6}$$

where $c_m = \sqrt{\frac{T}{\rho_m}}$ denotes for the speed of waves on membrane in which T and ρ_m are respectively the membrane tension and mass density. The quantities $\bar{P}^+$ and $\bar{P}^-$ on right hand side of (3.6) represent acoustic pressures in the regions lying at $\bar{z} > 0$ and $\bar{z} < 0$, respectively. Further, edge conditions on the membrane edges are imposed. These conditions define the type of physical connection as well ensure the uniqueness

of achieved solution. For sake of generality, the spring like conditions can be given as:

$$T\frac{\partial \bar{U}(\bar{x},\bar{y},\bar{t})}{\partial \bar{x}} - \bar{K}_1\bar{U}(\bar{x},\bar{y},\bar{t}) = 0, \quad \bar{x} = 0, \quad 0 < \bar{y} < \bar{b}, \tag{3.7}$$

$$T\frac{\partial \bar{U}(\bar{x},\bar{y},\bar{t})}{\partial \bar{x}} + \bar{K}_2\bar{U}(\bar{x},\bar{y},\bar{t}) = 0, \quad \bar{x} = \bar{a}, \quad 0 < \bar{y} < \bar{b}, \tag{3.8}$$

$$T\frac{\partial \bar{U}(\bar{x},\bar{y},\bar{t})}{\partial \bar{y}} - \bar{K}_3\bar{U}(\bar{x},\bar{y},\bar{t}) = 0, \quad \bar{y} = \bar{0}, \quad 0 < \bar{x} < \bar{a}, \tag{3.9}$$

$$T\frac{\partial \bar{U}(\bar{x},\bar{y},\bar{t})}{\partial \bar{y}} + \bar{K}_4\bar{U}(\bar{x},\bar{y},\bar{t}) = 0, \quad \bar{y} = \bar{a}, \quad 0 < \bar{x} < \bar{a}. \tag{3.10}$$

The membrane displacement $\bar{U}$ is related to fluid potential $\bar{\Phi}$ as:

$$\frac{\partial \bar{U}}{\partial \bar{t}} = \frac{\partial \bar{\Phi}}{\partial \bar{z}}. \tag{3.11}$$

Consider harmonic time dependence $e^{-i\omega\bar{t}}$, where ω is radiant frequency $\omega = 2\pi f$, then $\bar{P}, \bar{V}, \bar{U}$ and $\bar{\Phi}$ are related as:

$$\bar{P}(\bar{x},\bar{y},\bar{z},\bar{t}) = \bar{p}(\bar{x},\bar{y},\bar{z})e^{-i\omega\bar{t}}, \tag{3.12}$$

$$\bar{V}(\bar{x},\bar{y},\bar{z},\bar{t}) = \bar{v}(\bar{x},\bar{y},\bar{z})e^{-i\omega\bar{t}}, \tag{3.13}$$

$$\bar{\Phi}(\bar{x},\bar{y},\bar{z},\bar{t}) = \bar{\phi}(\bar{x},\bar{y},\bar{z})e^{-i\omega\bar{t}}, \tag{3.14}$$

and

$$\bar{U}(\bar{x},\bar{y},\bar{t}) = \bar{u}(\bar{x},\bar{y})e^{-i\omega\bar{t}}, \tag{3.15}$$

where $\bar{p}, \bar{v}, \bar{u}$ and $\bar{\phi}$ are time independent variables using (3.12) to (3.15) into (3.1) to (3.6), we get the following equations in harmonic time independent, variable.

- Helmholtz's equation:

$$\left[\frac{\partial^2}{\partial \bar{x}^2} + \frac{\partial^2}{\partial \bar{y}^2} + \frac{\partial^2}{\partial \bar{z}^2} + k^2\right]\bar{\phi}(\bar{x},\bar{y},\bar{z}) = 0. \tag{3.16}$$

- Relation of pressure, velocity and displacement with fluid potential:

$$\bar{p}(\bar{x},\bar{y},\bar{z}) = i\omega\rho\bar{\phi}(\bar{x},\bar{y},\bar{z}), \tag{3.17}$$

$$\bar{v}(\bar{x},\bar{y},\bar{z}) = \frac{\partial\bar{\phi}}{\partial\bar{x}}\hat{i} + \frac{\partial\bar{\phi}}{\partial\bar{y}}\hat{j} + \frac{\partial\bar{\phi}}{\partial\bar{z}}\hat{k}, \tag{3.18}$$

$$\bar{u}(\bar{x},\bar{y}) = \frac{i}{\omega}\frac{\partial\bar{\phi}}{\partial\bar{z}}. \tag{3.19}$$

- Rigid conditions at $\bar{x}=0, \quad \bar{x}=\bar{a}, \quad and \quad \bar{y}=0, \quad \bar{y}=\bar{b}$:

$$\frac{\partial\bar{\phi}}{\partial\bar{x}} = 0, \quad \bar{x}=0, \quad \bar{x}=\bar{a}, \quad 0<\bar{y}<\bar{b}, \tag{3.20}$$

$$\frac{\partial\bar{\phi}}{\partial\bar{y}} = 0, \quad \bar{y}=0, \quad \bar{y}=\bar{b}, \quad 0<\bar{x}<\bar{a}. \tag{3.21}$$

- Membrane condition at $\bar{z}=0, \quad 0\le\bar{x}\le\bar{a}, \quad 0\le\bar{y}\le\bar{b}$:

$$\frac{\partial^2\bar{u}}{\partial\bar{x}^2} + \frac{\partial^2\bar{u}}{\partial\bar{y}^2} + \frac{\omega^2}{c_m^2}\bar{u} = \frac{1}{T}(\bar{p}^+ - \bar{p}^-). \tag{3.22}$$

- Edge conditions at the edges of membrane:

$$T\frac{\partial\bar{u}(\bar{x},\bar{y})}{\partial\bar{x}} - \bar{K}_1\bar{u}(\bar{x},\bar{y}) = 0, \quad \bar{x}=0, \quad 0<\bar{y}<\bar{b}, \tag{3.23}$$

$$T\frac{\partial\bar{u}(\bar{x},\bar{y})}{\partial\bar{x}} + \bar{K}_2\bar{u}(\bar{x},\bar{y}) = 0, \quad \bar{x}=\bar{a}, \quad 0<\bar{y}<\bar{b}, \tag{3.24}$$

$$T\frac{\partial\bar{u}(\bar{x},\bar{y})}{\partial\bar{y}} - \bar{K}_3\bar{u}(\bar{x},\bar{y}) = 0, \quad \bar{y}=\bar{0}, \quad 0<\bar{x}<\bar{a}, \tag{3.25}$$

$$T\frac{\partial\bar{u}(\bar{x},\bar{y})}{\partial\bar{y}} + \bar{K}_4\bar{u}(\bar{x},\bar{y}) = 0, \quad \bar{y}=\bar{a}, \quad 0<\bar{x}<\bar{a}. \tag{3.26}$$

Now, we non-dimensionalize the above equations by using length scale k^{-1}, and time scale ω^{-1}, such that

$$\begin{cases} x = k\bar{x}, y = k\bar{y}, z = k\bar{z}, t = \omega\bar{t}, \\ u = k\bar{u}, \phi = \frac{k^2}{\omega}\bar{\phi}. \end{cases} \tag{3.27}$$

The differential operator in dimensional form are related to non-dimensional form as:

$$\frac{\partial}{\partial\bar{x}} = \frac{\partial}{\partial x}\frac{\partial x}{\partial\bar{x}} = k\frac{\partial}{\partial x}, \tag{3.28}$$

$$\frac{\partial^2}{\partial\bar{x}^2} = \frac{\partial}{\partial\bar{x}}(k\frac{\partial}{\partial x}) = k^2\frac{\partial^2}{\partial x^2}, \tag{3.29}$$

$$\frac{\partial}{\partial\bar{y}} = \frac{\partial}{\partial y}\frac{\partial y}{\partial\bar{y}} = k\frac{\partial}{\partial y}, \tag{3.30}$$

$$\frac{\partial^2}{\partial \bar{y}^2} = \frac{\partial}{\partial \bar{y}}(k\frac{\partial}{\partial y}) = k^2\frac{\partial^2}{\partial y^2}, \tag{3.31}$$

$$\frac{\partial}{\partial \bar{z}} = \frac{\partial}{\partial z}\frac{\partial z}{\partial \bar{z}} = k\frac{\partial}{\partial z}, \tag{3.32}$$

$$\frac{\partial^2}{\partial \bar{z}^2} = \frac{\partial}{\partial \bar{z}}(k\frac{\partial}{\partial z}) = k^2\frac{\partial^2}{\partial z^2}. \tag{3.33}$$

Now, we use the defined transformation (3.27) to make the equations dimensionless. The resulting dimensionless form of the equations of interest has been given below:

- Helmholtz's equation:

$$\left[\frac{\partial^2}{\partial x^2} + \frac{\partial^2}{\partial y^2} + \frac{\partial^2}{\partial z^2} + 1\right]\phi(x, y, z) = 0. \tag{3.34}$$

- Relation of pressure, velocity and displacement with fluid potential:

$$p(x, y, z) = \frac{i\omega^2\rho}{k^2}\phi(x, y, z), \tag{3.35}$$

$$v(x, y, z) = \frac{\omega}{k}\frac{\partial\phi}{\partial x}\hat{i} + \frac{\partial\phi}{\partial y}\hat{j} + \frac{\partial\phi}{\partial z}\hat{k}, \tag{3.36}$$

$$u(x, y) = \frac{i}{k}\frac{\partial\phi}{\partial z}. \tag{3.37}$$

- Rigid conditions at $x = 0, \quad x = a, \quad and \quad y = 0, \quad y = b$:

$$\frac{\partial\phi}{\partial x} = 0, \quad x = 0, \quad x = a, \quad 0 < y < b, \tag{3.38}$$

$$\frac{\partial\phi}{\partial y} = 0, \quad y = 0, \quad y = b, \quad 0 < x < a. \tag{3.39}$$

- Membrane condition at $z = 0, \quad 0 \le x \le a, \quad 0 \le y \le b$:

$$\left[\frac{\partial^2}{\partial x^2} + \frac{\partial^2}{\partial y^2} + \mu^2\right]\frac{\partial\phi}{\partial z} = \alpha(\phi^+ - \phi^-), \tag{3.40}$$

where $\mu = \frac{c}{c_m}$ and $\alpha = \frac{c^2\rho}{T}$ are dimensionless form of membrane wavenumber and fluid loading parameters, respectively.

- Edge conditions at the edges of membrane:

$$\frac{\partial u(x,y)}{\partial x} - K_1 u(x,y) = 0, \qquad x = 0, \qquad 0 < y < b, \tag{3.41}$$

$$\frac{\partial u(x,y)}{\partial x} + K_2 u(x,y) = 0, \qquad x = a, \qquad 0 < y < b, \tag{3.42}$$

$$\frac{\partial u(x,y)}{\partial \bar{y}} - K_3 u(x,y) = 0, \qquad y = 0, \qquad 0 < x < a, \tag{3.43}$$

$$\frac{\partial u(x,y)}{\partial y} + K_4 u(x,y) = 0, \qquad y = a, \qquad 0 < x < a, \tag{3.44}$$

where $k_1 = \frac{\bar{k}_1}{Tk}$, $k_2 = \frac{\bar{k}_2}{Tk}$, $k_3 = \frac{\bar{k}_3}{Tk}$ and $k_4 = \frac{\bar{k}_4}{Tk}$.

Let an incident wave strikes at membrane, a part is reflected in region-I while rest is transmitted into the region-II.

In order to analyze the reflection and transmission, we solve the governing boundary value problem (BVP) by using mode-matching technique. The solution is discussed in the next section.

3.2 Mode-Matching Solution

In this technique, first we apply the separation of variable method and determine the eigenfunction expansion of fluid potential in duct region-I and region-II.

For region-I, the Helmholtz's equation is

$$\left[\frac{\partial^2}{\partial x^2} + \frac{\partial^2}{\partial y^2} + \frac{\partial^2}{\partial z^2} + 1\right] \phi_1(x,y,z) = 0, \tag{3.45}$$

subject to the boundary conditions:

$$\frac{\partial \phi}{\partial x} = 0, \qquad x = 0, \qquad x = a, \tag{3.46}$$

$$\frac{\partial \phi}{\partial y} = 0, \qquad y = 0, \qquad y = b. \tag{3.47}$$

To solve (3.45), we assume the solution

$$\phi_1(x,y,z) = X_1(x) Y_1(y) Z_1(z). \tag{3.48}$$

On using (3.48) into (3.45), gives

$$\frac{X_1\,''(x)}{X_1(x)} + \frac{Y_1\,''(y)}{Y_1(y)} + 1 = -\frac{Z_1\,''(z)}{Z_1(z)} = \eta^2. \tag{3.49}$$

From (3.49), the solution of ordinary differential equation for $Z_1(z)$ is

$$Z_1(z) = c_1 e^{i\eta z} + c_2 e^{-i\eta z}, \tag{3.50}$$

where c_1 and c_2 are arbitrary constants. For $Y_1(y)$, the ordinary differential equation is

$$Y_1\,''(y) + \eta_y^2 Y_1(y) = 0, \quad \text{with} \quad \eta_y = \sqrt{1-\eta^2}. \tag{3.51}$$

The solution of equation (3.51), is

$$Y_1(y) = c_3 \cos(\eta_y y) + c_4 \sin(\eta_y y), \tag{3.52}$$

where c_3 and c_4 are arbitrary constants. By using (3.47) into (3.52), we may get

$$Y_1(y) = \cos\left(\frac{n\pi y}{b}\right), \quad \text{with} \quad \eta_y = \frac{n\pi}{b}, \tag{3.53}$$

whereas, for $X_1(x)$, the ordinary differential equation is

$$X_1\,''(x) + \eta_x^2 X_1(x) = 0, \quad \text{with} \quad \eta_x = \sqrt{1-\eta^2-\eta_y^2}. \tag{3.54}$$

The solution of (3.54), is

$$X_1(x) = c_5 \cos(\eta_x x) + c_6 \sin(\eta_x x), \tag{3.55}$$

where c_5 and c_6 are arbitrary constants. By using (3.46) into (3.55), we may get

$$X_1(x) = \cos\left(\frac{m\pi x}{a}\right), \quad \text{with} \quad \eta_x = \frac{m\pi}{a}. \tag{3.56}$$

From superposition principle, the total field potential in region-I can be written as:

$$\phi_1(x,y,z) = \sum_{m=0}^{\infty}\sum_{n=0}^{\infty}(A_{mn}e^{i\eta_{mn}z} + B_{mn}e^{-i\eta_{mn}z})\psi_{mn}(x,y), \tag{3.57}$$

where $\psi_{mn}(x, y)$ denotes the eigenfunction in region-I and its value is

$$\psi_{mn}(x, y) = \cos\left(\frac{m\pi x}{a}\right)\cos\left(\frac{n\pi y}{b}\right). \tag{3.58}$$

Here, η_{mn} represents the wave number corresponding to the $(mn)^{\text{th}}$ mode, and its value is given by

$$\eta_{mn} = \sqrt{1 - \left(\frac{m\pi}{a}\right)^2 - \left(\frac{n\pi}{b}\right)^2}. \tag{3.59}$$

Note that first term of right hand side of (3.57) gives the expression for $(mn)^{\text{th}}$ propagating mode towards positive direction and second term on right hand side stands for the $(mn)^{\text{th}}$ mode propagating in negative z-direction.

The coefficients A_{mn} and B_{mn} are amplitude of $(mn)^{\text{th}}$ propagating modes.

Likewise for region-II, we solve

$$\left[\frac{\partial^2}{\partial x^2} + \frac{\partial^2}{\partial y^2} + \frac{\partial^2}{\partial z} + 1\right]\phi_2(x, y, z) = 0, \tag{3.60}$$

subject to the boundary conditions:

$$\frac{\partial \phi_2}{\partial x} = 0, \qquad x = 0, \quad x = a, \tag{3.61}$$

$$\frac{\partial \phi_2}{\partial y} = 0, \qquad x = 0, \quad y = b. \tag{3.62}$$

To solve (3.60), consider

$$\phi_2(x, y, z) = X_2(x)Y_2(y)Z_2(z). \tag{3.63}$$

On using (3.63) into (3.60), we get

$$\frac{X_2\,''(x)}{X_2(x)} + \frac{Y_2\,''(y)}{Y_2(y)} + 1 = -\frac{Z_2\,''(z)}{Z_2(z)} = \eta^2. \tag{3.64}$$

From (3.64), the solution of ordinary differential equation for $Z_2(z)$ is

$$Z_2(z) = c_7 e^{i\eta z} + c_8 e^{-i\eta z}, \tag{3.65}$$

where c_7 and c_8 are arbitrary constants. For $Y_2(y)$, the ordinary differential equation is

$$Y_2\,''(y) + \eta_y^2 Y_2(y) = 0, \qquad \text{with} \qquad \eta_y = \sqrt{1-\eta^2}. \tag{3.66}$$

The solution of equation (3.66), is

$$Y_2(x) = c_9 \cos(\eta_y y) + c_{10} \sin(\eta_y y). \tag{3.67}$$

Here, c_9 and c_{10} are arbitrary constants. By using (3.62) into (3.67), we may get

$$Y_2(y) = \cos\left(\frac{n\pi y}{b}\right), \qquad \text{with} \qquad \eta_y = \frac{n\pi}{b}, \tag{3.68}$$

whereas, for $X_2(x)$, the ordinary differential equation is

$$X_2\,''(x) + \eta_x^2 X_2(x) = 0, \qquad \text{with} \qquad \eta_x = \sqrt{1-\eta^2-\eta_y^2}. \tag{3.69}$$

The solution of (3.69), is

$$X_2(x) = c_{11} \cos(\eta_x x) + c_{12} \sin(\eta_x x), \tag{3.70}$$

where c_{11} and c_{12} are arbitrary constants. By using (3.61) into (3.70), we may get

$$X_2(x) = \cos\left(\frac{m\pi x}{a}\right), \qquad \text{with} \qquad \eta_x = \frac{m\pi}{a}. \tag{3.71}$$

From superposition principle, the total field potential in region-II can be written as:

$$\phi_2(x,y,z) = \sum_{m=0}^{\infty}\sum_{n=0}^{\infty}(C_{mn}e^{i\eta_{mn}z} + D_{mn}e^{-i\eta_{mn}z})\psi_{mn}(x,y), \tag{3.72}$$

where $\psi_{mn}(x,y)$ denotes the eigenfunction in region-I and its value is

$$\psi_{mn}(x,y) = \cos\left(\frac{m\pi x}{a}\right)\cos(\frac{n\pi y}{b}). \tag{3.73}$$

Here, η_{mn} represents the wave number corresponding to the $(mn)^{\text{th}}$ mode, and its value is given by

$$\eta_{mn} = \sqrt{1 - \left(\frac{m\pi}{a}\right)^2 - \left(\frac{n\pi}{b}\right)^2}. \tag{3.74}$$

Note that $\{A_{mn}, B_{mn}, C_{mn}, D_{mn}\}$ are unknowns. We take the fundamental duct mode with unit amplitude from region-II to positive z-direction. Furthermore, we consider only transmission in region-II by setting $D_{mn} = 0$ in (3.72). Therefore, (3.57) and (3.72), respectively take the form:

$$\phi_1(x, y, z) = \sum_{m=0}^{\infty}\sum_{n=0}^{\infty}(A_{mn}e^{i\eta_{mn}z} + B_{mn}e^{-i\eta_{mn}z})\psi_{mn}(x, y), \tag{3.75}$$

and

$$\phi_2(x, y, z) = \sum_{m=0}^{\infty}\sum_{n=0}^{\infty}C_{mn}e^{i\eta_{mn}z}\psi_{mn}(x, y). \tag{3.76}$$

3.3 Dynamics of Membrane at Interface

The dynamical manner of membrane at interface $z = 0$, is given in equation of motion (3.40). We rewrite the membrane equation:

$$\nabla^2 u(x, y) + \mu^2 u(x, y) = \alpha(\phi_2 - \phi_1). \tag{3.77}$$

In order to find the solution of (3.77), using Galerkin approach which relies on the assumption of priori solution. Here, consider the solution in generalized Fourier series form as:

$$u(x, y) = \sum_{p=0}^{\infty}\sum_{q=0}^{\infty}D_{pq}\chi_{pq}(x, y), \tag{3.78}$$

where $\chi_{pq}(x, y)$ satisfies the eigenvalue problem associated with (3.77)

$$\nabla^2\chi_{pq} + \lambda_{pq}^2\chi_{pq} = 0, \tag{3.79}$$

with subject to boundary conditions:

$$\frac{\partial\chi_{pq}(x, y)}{\partial x} - k_1\chi_{pq}(x, y) = 0, \qquad x = 0, \tag{3.80}$$

$$\frac{\partial \chi_{pq}(x,y)}{\partial x} + k_2 \chi_{pq}(x,y) = 0, \qquad x = a, \tag{3.81}$$

$$\frac{\partial \chi_{pq}(x,y)}{\partial y} - k_3 \chi_{pq}(x,y) = 0, \qquad y = 0, \tag{3.82}$$

$$\frac{\partial \chi_{pq}(x,y)}{\partial y} + k_4 \chi_{pq}(x,y) = 0, \qquad y = b. \tag{3.83}$$

Note that D_{pq} is unknown that will be found through (3.77). However, to determine χ_{pq}, we solve eigenvalue problem given by (3.79) to (3.83). For sake of generality we assume

$$\chi_{pq} = X_p Y_q. \tag{3.84}$$

By using (3.84) into (3.79), we may get

$$\frac{X_p{}''}{X_p} = -\frac{Y_q{}''}{Y_q} - \lambda_{pq}^2 = -\gamma_p^2, \tag{3.85}$$

whereas, for $X_p(x)$, the ordinary differential equation is

$$X_p{}''(x) + \gamma_p^2 X_p(x) = 0. \tag{3.86}$$

The solution of (3.86), is

$$X_p = c_{13}\cos(\gamma_p x) + c_{14}\sin(\gamma_p x), \tag{3.87}$$

where c_{13} and c_{14} are arbitrary constants. By using (3.80) into (3.87), we may get

$$X_p = c_{14}\left(\frac{\gamma_p}{k_1}\cos(\gamma_p x) + \sin(\gamma_p x)\right). \tag{3.88}$$

On using (3.81) into (3.88), we obtain

$$c_{14}\left(\left(1 + \frac{k_2}{k_1}\right)\gamma_p \cos(\gamma_p a) + \left(k_2 - \frac{\gamma_p^2}{k_1}\right)\sin(\gamma_p a)\right) = 0. \tag{3.89}$$

For nontrivial solution, $c_{14} \neq 0$, then (3.89) can be rewritten as

$$\left(\left(1 + \frac{k_2}{k_1}\right)\gamma_p \cos(\gamma_p a) + \left(k_2 - \frac{\gamma_p^2}{k_1}\right)\sin(\gamma_p a)\right) = 0. \tag{3.90}$$

Here, the roots of equation (3.90), denoted as γ_p, will be obtained using numerical method like Newton - Raphson or Secant method. Hence

$$X_p = \frac{\gamma_p}{k_1}\cos(\gamma_p x) + \sin(\gamma_p x). \tag{3.91}$$

Here X_p are orthogonal, satisfying orthogonality relation that is

$$\int_0^a X_p X_l dx = \delta_{pl} E_l, \tag{3.92}$$

where

$$E_l = \int_0^a X_l^2 dx, \tag{3.93}$$

whereas, for $Y_q(y)$, the ordinary differential equation is

$$Y_q{}'' + \gamma_q^2 Y_q = 0, \quad \text{with} \quad \gamma_q = \sqrt{\lambda_{pq}^2 - \gamma_p^2}. \tag{3.94}$$

The solution of equation (3.94), is

$$Y_q = c_{15}\cos(\gamma_q y) + c_{16}\sin(\gamma_q y), \tag{3.95}$$

where c_{15} and c_{16} are arbitrary constants. By using (3.82) into (3.95), we obtain

$$Y_q = c_{16}\left(\frac{\gamma_q}{k_3}\cos(\gamma_q y) + \sin(\gamma_q y)\right). \tag{3.96}$$

On using (3.83) into (3.96), we obtain

$$c_{16}\left(\left(1 + \frac{k_4}{k_3}\right)\gamma_q\cos(\gamma_q b) + \left(k_4 - \frac{\gamma_q^2}{k_3}\right)\sin(\gamma_q b)\right) = 0. \tag{3.97}$$

For nontrivial solution, $c_{16} \neq 0$, then (3.97) can be written as:

$$\left(\left(1 + \frac{k_4}{k_3}\right)\gamma_q\cos(\gamma_q b) + \left(k_4 - \frac{\gamma_q^2}{k_3}\right)\sin(\gamma_q b)\right) = 0. \tag{3.98}$$

Here, the roots of equation (3.98), denoted as γ_q, will be obtained using numerical method like Newton - Raphson or Secant method. Hence

$$Y_q = \frac{\gamma_q}{k_2}\cos(\gamma_q y) + \sin(\gamma_q y). \tag{3.99}$$

Here, Y_q are orthogonal, satisfying orthogonality relation that is

$$\int_0^a Y_q Y_m dy = \delta_{qm} F_m, \tag{3.100}$$

where

$$F_m = \int_0^b Y_m^2 dy. \tag{3.101}$$

In order to show orthogonality we reconsider (3.84), which is

$$\chi_{pq} = X_p Y_q. \tag{3.102}$$

On multiplying by χ_{lm} and integrating over $0 < x < a$ and $0 < y < b$, we may get

$$\int_0^a \int_0^b \chi_{pq}\chi_{lm} dxdy = \Gamma_{lm}\delta_{pl}\delta_{qm}. \tag{3.103}$$

By using orthogonality relation (3.103), after simplification yields

$$\Gamma_{lm} = E_l F_m. \tag{3.104}$$

By using (3.75),(3.76) and (3.78) into (3.77), we may get

$$\sum_{p=0}^{\infty}\sum_{q=0}^{\infty} D_{pq}(\mu^2 - \lambda_{pq}^2)\chi_{pq} = \alpha \sum_{m=0}^{\infty}\sum_{n=0}^{\infty}(A_{mn} + B_{mn} - C_{mn})\psi_{mn}. \tag{3.105}$$

On multiplying with χ_{lm} and integrating over $0 < x < a$ and $0 < y < b$, we may get

$$D_{lm} = \frac{\alpha}{(\mu^2 - \lambda_{lm}^2)\Gamma_{lm}} \sum_{r=0}^{\infty}\sum_{n=0}^{\infty}(A_{rn} + B_{rn} - C_{rn})\Delta_{rnlm}. \tag{3.106}$$

By using orthogonality relation (3.106), and simplifying, we get

$$\Delta_{rnlm} = \int_0^a \int_0^b \chi_{lm}\psi_{rn} dxdy. \tag{3.107}$$

Accordingly, for region-I, at $z = 0$, we have

$$\frac{\partial \phi_1}{\partial z} = u(x, y). \tag{3.108}$$

By using (3.75) and (3.78) into (3.108), we may get

$$i \sum_{m=0}^{\infty} \sum_{n=0}^{\infty} (A_{mn} - B_{mn}) \eta_{mn} \psi_{mn}(x, y) = \sum_{p=0}^{\infty} \sum_{q=0}^{\infty} D_{pq} \chi_{pq}. \tag{3.109}$$

Multiplying by ψ_{gj} with (3.109) and integrating over $0 < x < a$ and $0 < y < b$, we may get

$$A_{gj} - B_{gj} = \frac{1}{i \eta_{gj} \triangle_{gj}} \sum_{p} \sum_{q} D_{pq} \Delta_{gjpq}, \tag{3.110}$$

where

$$\Delta_{gjpq} = \int_0^a \int_0^b \psi_{gj} \chi_{pq} dx dy. \tag{3.111}$$

Similarly, for region-II, at $z = 0$, we have

$$\frac{\partial \phi_2}{\partial z} = u(x, y). \tag{3.112}$$

By using (3.76) and (3.78) into (3.112), we may get

$$i \sum_{m=0}^{\infty} \sum_{n=0}^{\infty} C_{mn} \eta_{mn} \psi_{mn}(x, y) = \sum_{p=0}^{\infty} \sum_{q=0}^{\infty} D_{pq} \chi_{pq}. \tag{3.113}$$

By using orthogonality relation, after some mathematical rearrangements, it is found that

$$C_{gj} = \frac{1}{i \eta_{gj} \triangle_{gj}} \sum_{p} \sum_{q} D_{pq} \bigwedge_{gjpq}, \tag{3.114}$$

where

$$\bigwedge_{gjpq} = \int_0^a \int_0^b \psi_{gj} \chi_{pq} dx dy. \tag{3.115}$$

3.4 Numerical Results

This section presents a numerical solution to the problem examined in the chapter, where the system is truncated upto N terms. The numerical computations are performed in software *MATHEMATICA* by fixing the relevant parameters as: membrane dimensions $\bar{a} = 0.1\text{m}$, $\bar{b} = 0.1\text{m}$, density of air $\rho = 1.2\text{kg}/m^3$, sound speed in air $c = 343.5\text{m/s}$, tension $T = 50\text{N}$, membrane mass density $\rho_m = 0.17\text{kg}/m^3$, frequency $f = 100\text{Hz}$ and spring constants $\bar{k}_1 = \bar{k}_2 = \bar{k}_3 = \bar{k}_4 = 1$.

In Figures 3.2 to 3.7, the dimensionless modes of membrane at $\psi_{00}(x, y)$, $\psi_{01}(x, y)$, $\psi_{10}(x, y)$, $\psi_{55}(x, y)$ and $\psi_{99}(x, y)$ against x and y at $z = 0$ are shown and Figures 3.8 to 3.13, the dimensionless modes of membrane of eigenfunction in 3-dimension at $\chi_{00}(x, y)$, $\chi_{01}(x, y)$, $\chi_{10}(x, y)$, $\chi_{11}(x, y)$, $\chi_{55}(x, y)$ and $\chi_{99}(x, y)$ against x and y at $z = 0$ are shown.

In Fig. 3.2, the (00) mode shows that the entire membrane moves up and down uniformly, without any nodal lines (regions of zero displacement). This means that at any given time, the displacement is the same across the entire membrane.

In a density plot, colours typically represent amplitude variations. The black colour suggests that the amplitude does not change. The absence of variation confirms that this is the (00) mode, where the displacement is constant.

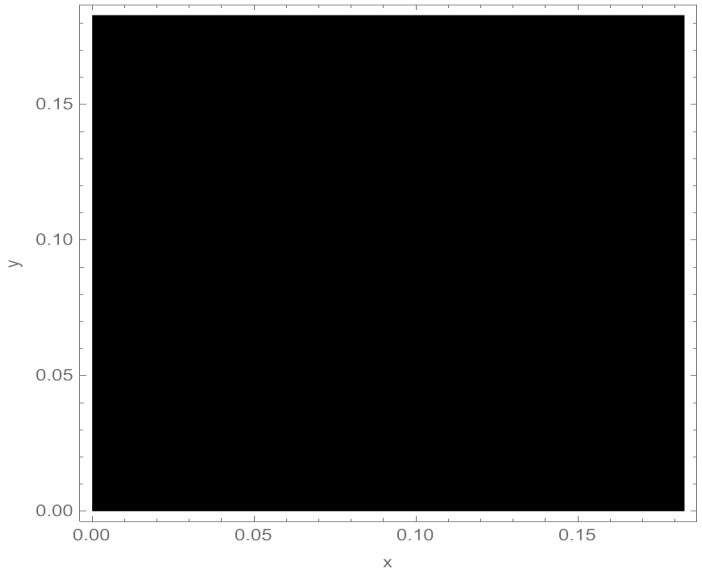

FIGURE 3.2: The dimensionless fluid mode at $\psi_{00}(x, y)$ against x and y, where $\bar{a} = \bar{b} = 0.1\text{m}$, and $N = 20$ terms

In Fig. 3.3, the (01) mode shows that the membrane vibrates in a way where the displacement varies smoothly in the vertical direction, but remains constant in the horizontal direction.

The colour gradient represents displacement values, white and yellow at the bottom indicates maximum positive displacement while the black at the top indicates the maximum negative displacement.

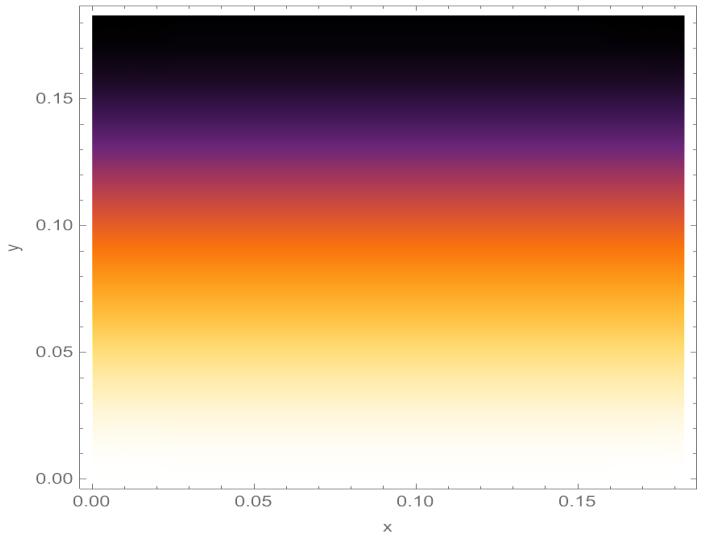

FIGURE 3.3: The dimensionless fluid mode at $\psi_{01}(x, y)$ against x and y, where $\bar{a} = \bar{b} = 0.1$m, and N $= 20$ terms

In Fig. 3.4, the (10) mode describes a standing wave pattern, where the displacement changes along the hoizantal direction, while uniform along the vertical direction.

White and yellow on the left indicates the maximum positive displacement and black on the right indicates maximum negative displacement.

In Fig. 3.5, the density plot of membrane (11) mode of a vibrating membrane indicates where the displacement varies in both horizontal and vertical directions. Bright (yellow and white) regions correspond to maximum displacement called antinodes, where the membrane moves most. Dark (purple and black) regions represent nodes, where the displacement is nearly zero. Gradient transitions between colors indicate areas of intermediate displacement.

In Fig. 3.6, the (55) mode describes a displacement varies in both the x and y directions with five oscillations. Bright (white and yellow) regions correspond to areas of maximum displacement (antinodes).

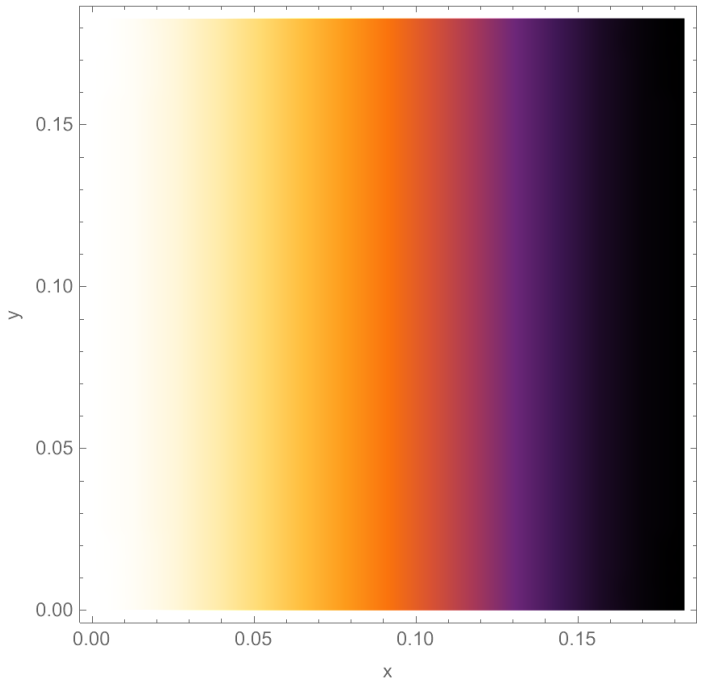

FIGURE 3.4: The dimensionless fluid mode at $\psi_{10}(x, y)$ against x and y, where $\bar{a} = \bar{b} = 0.1$m, and N = 20 terms

Dark (purple and black) regions correspond to areas of zero displacement (nodes). The repeating square-like pattern suggests a combination of sinusoidal oscillations.

In Fig. 3.7, the modes of vibration correspond to standing wave patterns, where certain points on the membrane remain stationary (nodes), while others oscillate between maximum and minimum displacement values. The black and dark purple colour represents minimum displacement (negative peaks), where the membrane moves the farthest in one direction.

The white and yellow colour represents maximum displacement (positive peaks), where the membrane moves the farthest in the opposite direction.

Orange Shades indicate intermediate values between the peaks and troughs.

In Fig. 3.8, the displacement varies in both the x and y directions with nine oscillations.. Since both n and m are 9, the membrane forms a 9×9 grid of nodal lines. Alternating bright and dark regions represent antinodes (max displacement) and nodes (zero displacement). Fine grid-like pattern confirms a high-frequency mode.

In Fig. 3.9, the (00) mode is the simplest and lowest-frequency vibration mode of a membrane. In this mode, the entire membrane moves up and down in unison, without

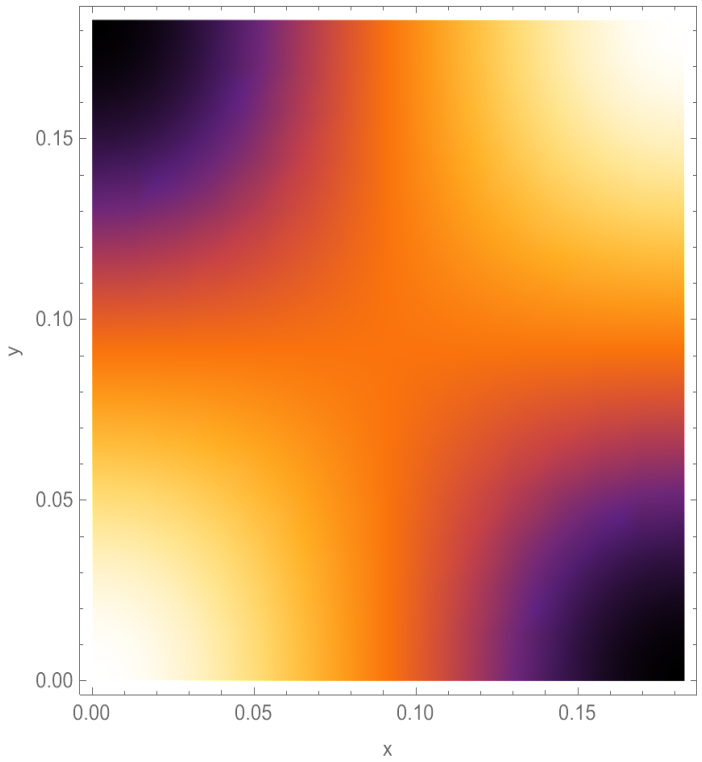

FIGURE 3.5: The dimensionless fluid mode at $\psi_{11}(x, y)$ against x and y, where $\bar{a} = \bar{b} = 0.1$m, and N = 20 terms

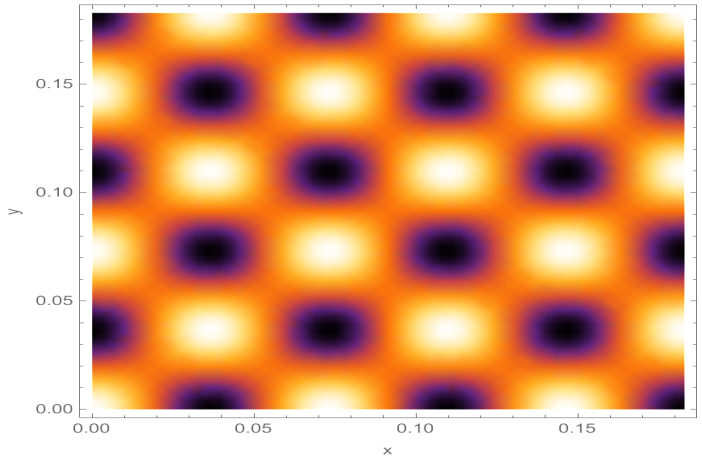

FIGURE 3.6: The dimensionless fluid mode at $\psi_{55}(x, y)$ against x and y, where $\bar{a} = \bar{b} = 0.1$m, and N = 20 terms

any internal oscillation patterns. The highest displacement occurs at the center, while it decreases towards the edges, where the boundary conditions force the displacement to be zero. The bright yellow and white areas indicate maximum displacement while the dark purple and black areas represent regions with minimal displacement.

In Fig. 3.10, the plot represents the (01) mode of a vibrating membrane. This mode exhibits a single oscillation along the y-axis, while remaining uniform along

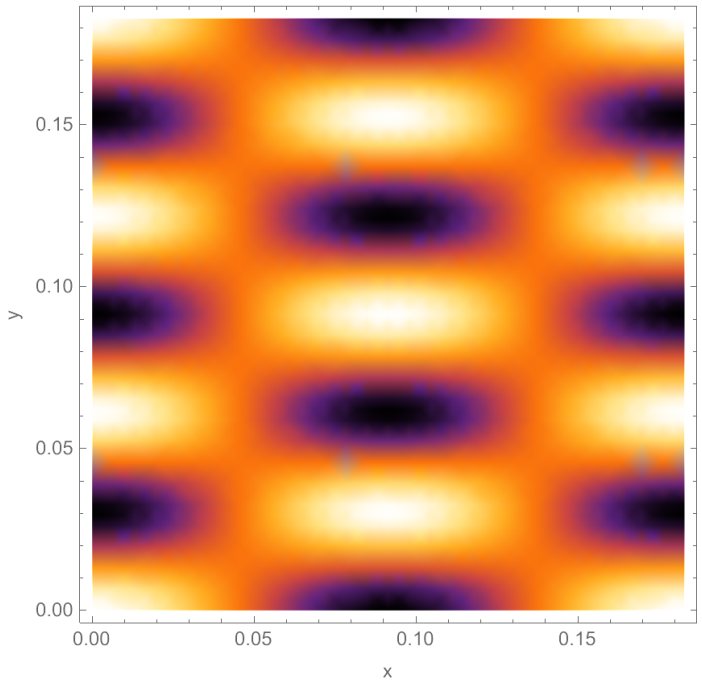

FIGURE 3.7: The dimensionless fluid mode at $\psi_{26}(x, y)$ against x and y, where $\bar{a} = \bar{b} = 0.1$m, and N = 20 terms

the x-axis, forming a standing wave in one direction. The bright regions represent maximum displacement(antinodes) and the dark regions represent zero displacement (nodes, fixed boundaries).

In Fig. 3.11, the (10) mode represents the simplest one-dimensional oscillation in a 2D membrane. The 3D plot helps visualize displacement variations, with color gradients highlighting oscillation intensity. The colours range from black (low values) to yellow (high values), indicating varying displacements or pressures.

In Fig. 3.12, In this case, it would show the mode (11), which corresponds to one oscillation along x direction and one along y direction. In this plot bright yellow and white indicates the maximum positive displacement while orange and purple indicates intermediate values and black and dark colours indicate maximum negative displacement.

In Fig. 3.13, the surface exhibits repetitive wave-like patterns in both the x and y directions, indicating a high frequency oscillation. The highest and lowest points in the plot correspond to antinodes (regions of maximum oscillation), while flat or intersecting regions indicate nodal lines where there is no motion. The bright yellow

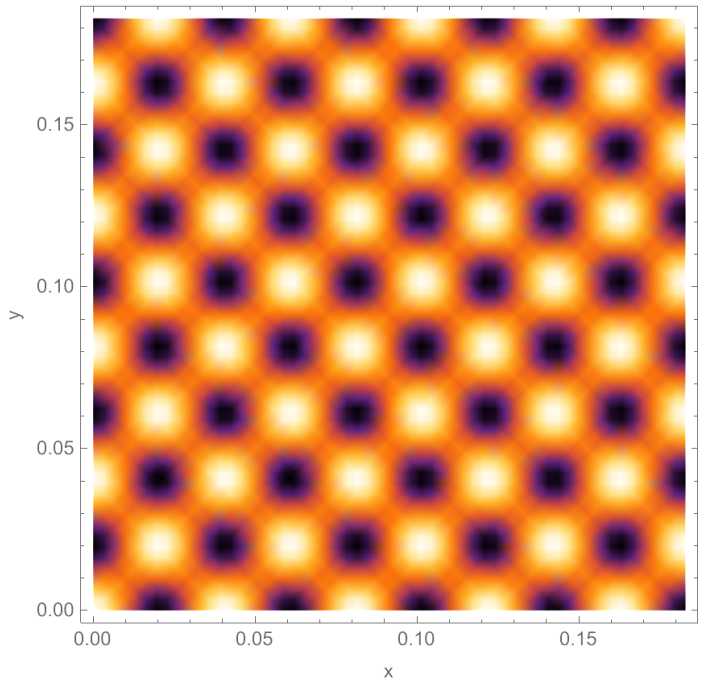

FIGURE 3.8: The dimensionless fluid mode at $\psi_{99}(x, y)$ against x and y, where $\bar{a} = \bar{b} = 0.1$m, and N = 20 terms

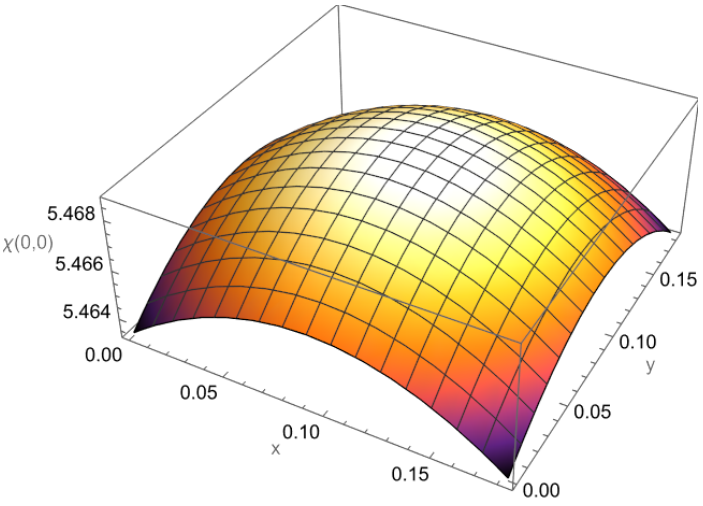

FIGURE 3.9: The dimensionless fluid mode of membrane of eigenfunction in 3D $\chi_{00}(x, y)$ against x and y, where $\bar{a} = \bar{b} = 0.1$m, and N = 20 terms

and white areas represent the highest positive displacements while the dark purple and black areas represent the lowest negative displacements.

In Fig. 3.14, the mode number increases, the wave pattern becomes more intricate. The bright yellow and white areas correspond to maximum positive displacement (peaks) while the dark purple and black areas represent maximum negative displacement (valleys) and the regions where the wave crosses zero displacement (flat parts) correspond to nodal lines, where no movement occurs.

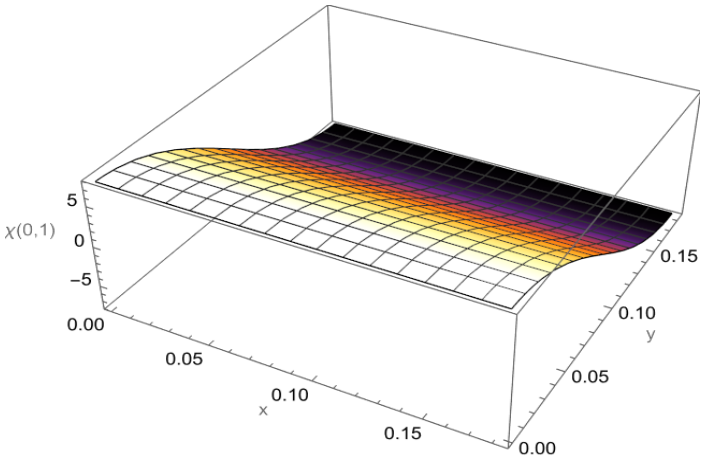

FIGURE 3.10: The dimensionless fluid mode of membrane of eigenfunction in 3D $\chi_{01}(x, y)$ against x and y, where $\bar{a} = \bar{b} = 0.1$m, and N = 20 terms

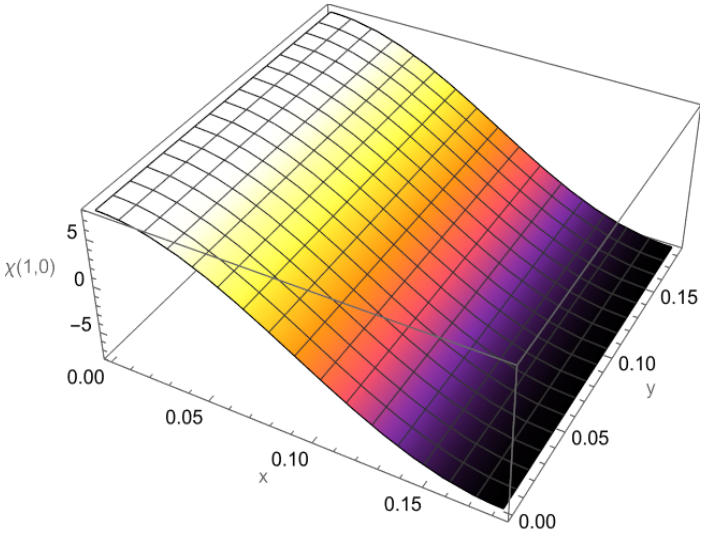

FIGURE 3.11: The dimensionless fluid mode of membrane of eigenfunction in 3D $\chi_{10}(x, y)$ against x and y, where $\bar{a} = \bar{b} = 0.1$m, and N = 20 terms

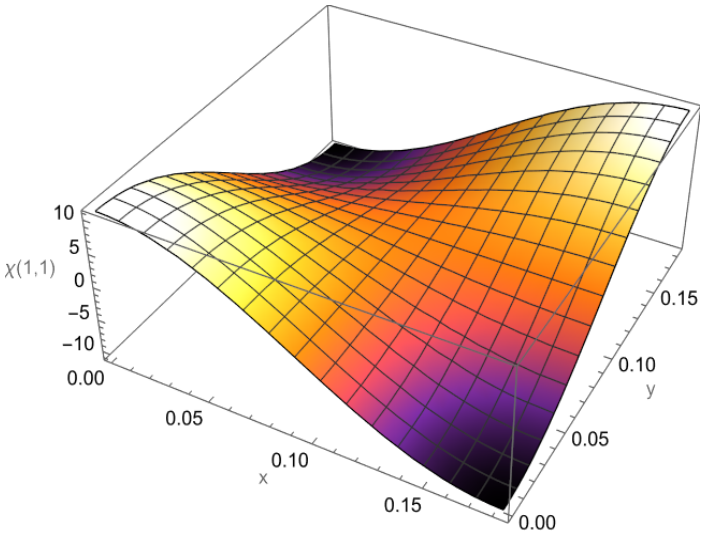

FIGURE 3.12: The dimensionless fluid mode of membrane of eigenfunction in 3D $\chi_{11}(x, y)$ against x and y, where $\bar{a} = \bar{b} = 0.1$m, and N = 20 terms

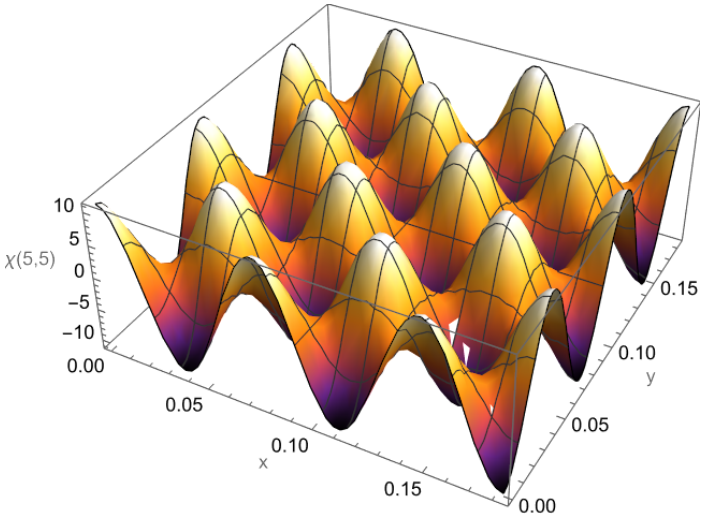

FIGURE 3.13: The dimensionless fluid mode of membrane of eigenfunction in 3D $\chi_{55}(x, y)$ against x and y, where $\bar{\mathrm{a}} = \bar{\mathrm{b}} = 0.1\mathrm{m}$, and $\mathrm{N} = 20$ terms

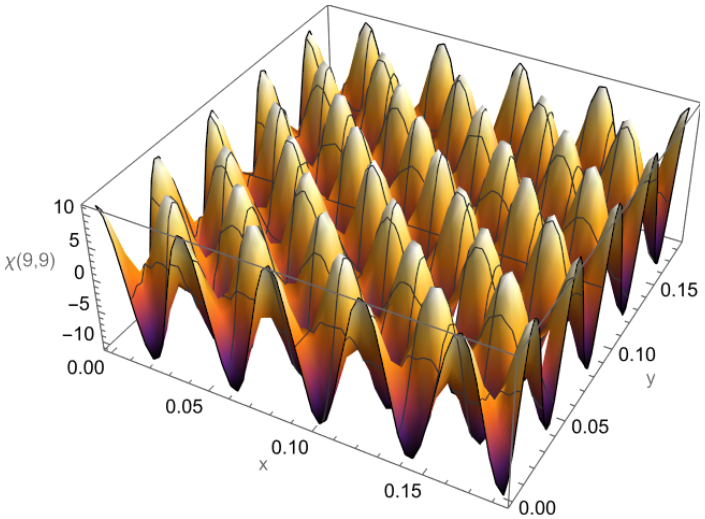

FIGURE 3.14: The dimensionless fluid mode of membrane of eigenfunction in 3D $\chi_{99}(x, y)$ against x and y, where $\bar{\mathrm{a}} = \bar{\mathrm{b}} = 0.1\mathrm{m}$, and $\mathrm{N} = 20$ terms

Chapter 4

Scattering of Acoustic Wave from a Rectangular Membrane in 3D Waveguide

In this chapter, the Scattering of acoustic wave from a rectangular membrane in 3-dimensional waveguide is discussed. The chapter is arranged as follows: Section 4.1 contains, the Scattering of acoustic wave from a rectangular membrane backed by rigid wall. Section 4.2 contains, the Galerkin's formulation to model the membrane response velocity condition for symmetric modes. The numerical results and discussion are given in Section 4.3. In Section 4.4 contains, the scattering of acoustic wave from a rectangular membrane backed by soft wall. The Galerkin's formulation to model the membrane response velocity condition for antisymmetric modes is given in Section 4.5. The numerical results and discussion are given in Section 4.6.

4.1 Scattering of Acoustic Wave from a Rectangular Membrane Backed by Rigid wall

Consider a duct mode incident on a membrane sheet of area "ab" located at $z = -\ell$.

There is a rigid wall located at $z = 0$, and incident modes is coming from $z < -\ell$. The geometry of waveguide is as shown in Fig. 4.1.

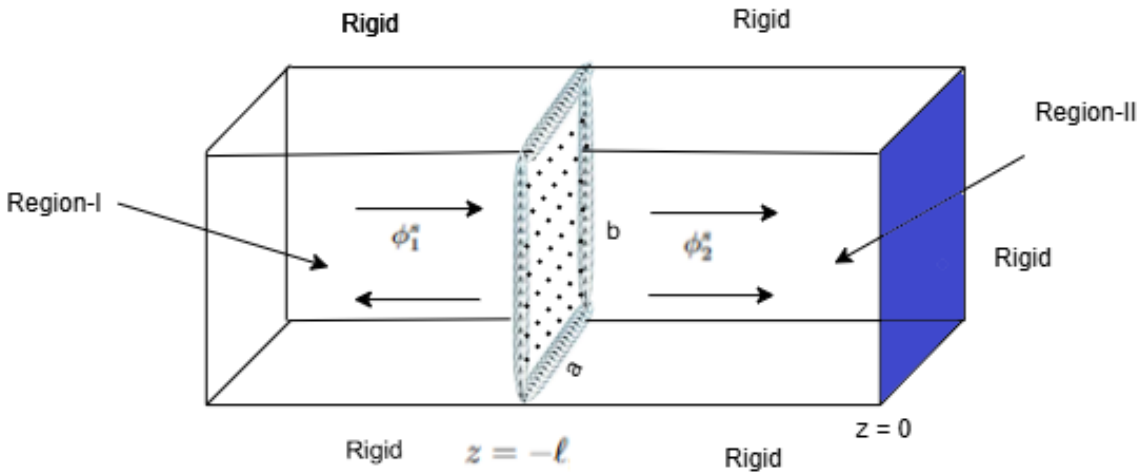

FIGURE 4.1: The physical configuration of waveguide

The fluid potentials in region-I and region-II can be expressed as:

$$\phi^s(x,y) = \begin{cases} \phi_1^s(x,y) & z < -\ell, \\ \phi_2^s(x,y) & z > -\ell, \end{cases} \tag{4.1}$$

where superscript "s" represent symmetric regions. These satisfies the Helmholtz's equation along with rigid boundary conditions. These governing equations are:

$$\{\nabla^2 + k^2\}\phi^s = 0, \tag{4.2}$$

$$\frac{\partial \phi_1^s}{\partial x} = 0, \qquad x = 0, \qquad x = a, \qquad 0 < y < b, \tag{4.3}$$

$$\frac{\partial \phi_2^s}{\partial y} = 0, \qquad x = 0, \qquad x = b, \qquad 0 < x < a. \tag{4.4}$$

The fluid potentials can be written in eigenfunction expansion form that is:

$$\phi_1^s(x,y,z) = \sum_{m=0}^{\infty}\sum_{n=0}^{\infty}\left(A_{mn}^s e^{i\eta_{mn}(z+l)} + B_{mn}^s e^{-i\eta_{mn}(z+l)}\right)\psi_{mn}(x,y), \tag{4.5}$$

and

$$\phi_2^s(x,y,z) = \sum_{m=0}^{\infty}\sum_{n=0}^{\infty}\left(C_{mn}^s e^{i\eta_{mn}z} + D_{mn}^s e^{-i\eta_{mn}z}\right)\psi_{mn}(x,y). \tag{4.6}$$

But as at $z = 0$, there exist a rigid wall that gives

$$\frac{\partial \phi_2^s}{\partial z} = 0, \qquad z = 0. \tag{4.7}$$

By using (4.6) into (4.7), we may get

$$\sum_{m=0}^{\infty}\sum_{n=0}^{\infty}(C_{mn}^s - D_{mn}^s)\eta_{mn}\psi_{mn}(x,y) = 0, \tag{4.8}$$

simplification leads to

$$C_{mn}^s = D_{mn}^s. \tag{4.9}$$

By using the value of D_{mn}, from (4.9) into (4.6), we find

$$\phi_2^s(x,y,z) = \sum_{m=0}^{\infty}\sum_{n=0}^{\infty} 2C_{mn}^s \cos(\eta_{mn} z)\psi_{mn}(x,y). \tag{4.10}$$

Here the coefficient C_{mn}^s and B_{mn}^s are unknowns once A_{mn}^s is provided to the system for excitation of duct modes. As there lies a membrane at $z = -\ell$, we consider its dynamics using Galerkin method to find the unknown amplitudes.

4.2 Galerkin Formulation for Membrane Dynamics

The dynamical response of membrane at interface $z = -\ell$, can be given as:

$$\nabla^2 u^s(x,y) + \mu^2 u^s(x,y) = \alpha(\phi_2^s - \phi_1^s), \tag{4.11}$$

subject to the boundary conditions:

$$\frac{\partial u^s(x,y)}{\partial x} - k_1 u^s(x,y) = 0, \qquad x = 0, \tag{4.12}$$

$$\frac{\partial u^s(x,y)}{\partial x} + k_2 u^s(x,y) = 0, \qquad x = a, \tag{4.13}$$

$$\frac{\partial u^s(x,y)}{\partial y} - k_3 u^s(x,y) = 0, \qquad y = 0, \tag{4.14}$$

$$\frac{\partial u^s(x,y)}{\partial y} + k_4 u^s(x,y) = 0, \qquad y = b. \tag{4.15}$$

Here, we assume the solution in generalized Fourier series form as:

$$u^s(x,y) = \sum_{p=0}^{\infty}\sum_{q=0}^{\infty} J^s_{pq}\chi^s_{pq}(x,y), \tag{4.16}$$

where $\chi^s_{pq}(x,y)$ satisfies the eigenvalue problem associated with (4.11)

$$\nabla^2\chi^s_{pq} + \lambda^2_{pq}\chi^s_{pq} = 0, \tag{4.17}$$

with subject to boundary conditions:

$$\frac{\partial \chi^s_{pq}(x,y)}{\partial x} - k_1\chi^s_{pq}(x,y) = 0, \qquad x = 0, \tag{4.18}$$

$$\frac{\partial \chi^s_{pq}(x,y)}{\partial x} + k_2\chi^s_{pq}(x,y) = 0, \qquad x = a, \tag{4.19}$$

$$\frac{\partial \chi^s_{pq}(x,y)}{\partial y} - k_3\chi^s_{pq}(x,y) = 0, \qquad y = 0, \tag{4.20}$$

$$\frac{\partial \chi^s_{pq}(x,y)}{\partial y} + k_4\chi^s_{pq}(x,y) = 0, \qquad y = b. \tag{4.21}$$

Note that J^s_{pq} is unknown that will be found through (4.11).

However, to determine χ^s_{pq}, we solve eigenvalue problem given by (4.17) to (4.21). For sake of generality we assume

$$\chi^s_{pq} = X_p Y_q. \tag{4.22}$$

By using (4.22) into (4.17), we may get

$$\frac{X_p{}''}{X_p} = -\frac{Y_q{}''}{Y_q} - \lambda^2_{pq} = -\gamma^2_p, \tag{4.23}$$

whereas, for $X_p(x)$, the ordinary differential equation is

$$X_p{}''(x) + \gamma^2_p X_p(x) = 0. \tag{4.24}$$

The solution of (4.24), is

$$X_p = c_{17}\cos(\gamma_p x) + c_{18}\sin(\gamma_p x), \tag{4.25}$$

where c_{17} and c_{18} are arbitrary constants. By using (4.18) into (4.25), we may get

$$X_p = c_{18}\left(\frac{\gamma_p}{k_1}\cos(\gamma_p x) + \sin(\gamma_p x)\right). \tag{4.26}$$

On using (4.19) into (4.26), we obtain

$$c_{18}\left(\left(1+\frac{k_2}{k_1}\right)\gamma_p\cos(\gamma_p a) + \left(k_2 - \frac{\gamma_p^2}{k_1}\right)\sin(\gamma_p a)\right) = 0. \tag{4.27}$$

For nontrivial solution, $c_{18} \neq 0$, then (4.27) can be rewritten as

$$\left(\left(1+\frac{k_2}{k_1}\right)\gamma_p\cos(\gamma_p a) + \left(k_2 - \frac{\gamma_p^2}{k_1}\right)\sin(\gamma_p a)\right) = 0. \tag{4.28}$$

Here, the roots of equation (4.28), denoted as γ_p, will be obtained using numerical method like Newton - Raphson or Secant method. Hence

$$X_p = \frac{\gamma_p}{k_1}\cos(\gamma_p x) + \sin(\gamma_p x). \tag{4.29}$$

Here, X_p are orthogonal, satisfying orthogonality relation that is

$$\int_0^a X_p X_l dx = \delta_{pl} E_l, \tag{4.30}$$

where

$$E_l = \int_0^a X_l^2 dx, \tag{4.31}$$

whereas, for $Y_q(y)$, the ordinary differential equation is

$$Y_q{}'' + \gamma_q^2 Y_q = 0, \quad \text{with} \quad \gamma_q = \sqrt{\lambda_{pq}^2 - \gamma_p^2}. \tag{4.32}$$

The solution of equation (4.32), is

$$Y_q = c_{19}\cos(\gamma_q y) + c_{20}\sin(\gamma_q y), \tag{4.33}$$

where c_{19} and c_{20} are arbitrary constants. By using (4.20), into (4.33) we obtain

$$Y_q = c_{20}\left(\frac{\gamma_q}{k_3}\cos(\gamma_q y) + \sin(\gamma_q y)\right). \tag{4.34}$$

On using (4.21) into (3.34), we obtain

$$c_{20}\left(\left(1+\frac{k_4}{k_3}\right)\gamma_q\cos(\gamma_q b) + \left(k_4 - \frac{\gamma_q^2}{k_3}\right)\sin(\gamma_q b)\right) = 0. \tag{4.35}$$

For nontrivial solution, $c_{20} \neq 0$, then (4.35) can be written as:

$$\left(\left(1+\frac{k_4}{k_3}\right)\gamma_q\cos(\gamma_q b) + \left(k_4 - \frac{\gamma_q^2}{k_3}\right)\sin(\gamma_q b)\right) = 0. \tag{4.36}$$

Here, the roots of equation (4.36), denoted as γ_q, will be obtained using numerical method like Newton - Raphson or Secant method. Hence

$$Y_q = \frac{\gamma_q}{k_2}\cos(\gamma_q y) + \sin(\gamma_q y). \tag{4.37}$$

Here, Y_q are orthogonal, satisfying orthogonality relation that is

$$\int_0^a Y_q Y_m dy = \delta_{qm} F_m, \tag{4.38}$$

where

$$F_m = \int_0^b Y_m^2 dy. \tag{4.39}$$

In order to show orthogonality we reconsider (4.22), which is

$$\chi_{pq}^s = X_p Y_q. \tag{4.40}$$

On multiplying by χ_{lm}^s and integrating over $0 < x < a$ and $0 < y < b$, we may get

$$\int_0^a \int_0^b \chi_{pq}^s \chi_{lm}^s dx dy = \Gamma_{lm}\delta_{pl}\delta_{qm}. \tag{4.41}$$

By using orthogonality relation (4.41), and simplifying, we get

$$\Gamma_{lm} = E_l F_m. \tag{4.42}$$

The value of χ^s_{pq}, is

$$\chi^s_{pq} = \left(\frac{\gamma_p}{k_1}\cos(\gamma_p x) + \sin(\gamma_p x)\right)\left(\frac{\gamma_q}{k_2}\cos(\gamma_q y) + \sin(\gamma_q y)\right). \tag{4.43}$$

On multiplying we get the following form

$$\begin{aligned}\chi^s_{pq} = {} & \frac{\gamma_p\gamma_q}{k_1k_2}\cos(\gamma_p x)\cos(\gamma_q y) + \frac{\gamma_p}{k_1}\cos(\gamma_p x)\sin(\gamma_q y) + \frac{\gamma_q}{k_2}\cos(\gamma_q y)\sin(\gamma_p x) \\ & + \sin(\gamma_p x)\sin(\gamma_q y).\end{aligned} \tag{4.44}$$

By using (4.5),(4.10) and (4.16) into (4.11), leads to

$$\sum_{p=0}^{\infty}\sum_{q=0}^{\infty} J^s_{pq}(\mu^2 - \lambda^2_{pq})\chi_{pq} = \alpha\sum_{m=0}^{\infty}\sum_{n=0}^{\infty}(A^s_{mn} + B^s_{mn} - 2C^s_{mn}\cos(\eta_{mn}l))\psi_{mn}. \tag{4.45}$$

On multiplying with χ^s_{lm} and integrating over $0 < x < a$ and $0 < y < b$, we may get

$$J^s_{lm} = \frac{\alpha}{(\mu^2 - \lambda^2_{lm})\Gamma_{lm}}\sum_{r=0}^{\infty}\sum_{n=0}^{\infty}(A^s_{rn} + B^s_{rn} - 2C^s_{rn}\cos(\eta_{rn}l))\Delta_{rnlm}. \tag{4.46}$$

By using orthogonality relation (4.46), and simplifying, we get

$$\Delta_{rnlm} = \int_0^a\int_0^b \chi^s_{lm}\psi_{rn}dxdy. \tag{4.47}$$

Accordingly, for region-I, at $z = -\ell$, we have

$$\frac{\partial\phi^s_1}{\partial z} = u^s(x, y). \tag{4.48}$$

By using (4.5) and (4.16) into (4.48), becomes

$$i\sum_{m=0}^{\infty}\sum_{n=0}^{\infty}(A^s_{mn} - B^s_{mn})\eta_{mn}\psi_{mn}(x, y) = \sum_{p=0}^{\infty}\sum_{q=0}^{\infty} J^s_{pq}\chi^s_{pq}. \tag{4.49}$$

Multiplying by ψ_{gj} with (4.49) and integrating over $0 < x < a$ and $0 < y < b$, we may get

$$A^s_{gj} - B^s_{gj} = \frac{1}{i\eta_{gj}\triangle_{gj}} \sum_{p=0}^{\infty}\sum_{q=0}^{\infty} J^s_{pq}\Delta_{gjpq}, \tag{4.50}$$

where

$$\Delta_{gjpq} = \int_0^a \int_0^b \psi_{gj}\chi^s_{pq} dxdy. \tag{4.51}$$

Similarly, for region-II, at $z = -\ell$, we have

$$\frac{\partial \phi^s_2}{\partial z} = u^s(x, y). \tag{4.52}$$

By using (4.10) and (4.16) into (4.52), we may get

$$\sum_{m=0}^{\infty}\sum_{n=0}^{\infty} 2C^s_{mn}\eta_{mn}\sin(\eta_{mn}l)\psi_{mn}(x, y) = \sum_{p=0}^{\infty}\sum_{q=0}^{\infty} J^s_{pq}\chi^s_{pq}. \tag{4.53}$$

By using orthogonality relation, after some mathematical rearrangements, it is found that

$$C^s_{gj} = \frac{1}{2\sin(\eta_{gj}l)\eta_{gj}\triangle_{gj}} \sum_{p=0}^{\infty}\sum_{q=0}^{\infty} J^s_{pq} \bigwedge_{gjpq}, \tag{4.54}$$

where

$$\bigwedge_{gjpq} = \int_0^a \int_0^b \psi_{gj}\chi^s_{pq} dxdy. \tag{4.55}$$

4.3 Numerical Results for Rigid Wall

Here, the problem of a rigid-backed cavity is solved numerically by truncating up to N terms. The numerical computations are carried out using the software *MATHEMATICA*, with the following parameter values: membrane dimensions $\bar{a} = 0.2\,\text{m}$, $\bar{b} = 0.3\,\text{m}$; cavity length $\bar{L} = 0.1\,\text{m}$; air density $\rho = 1.2\,\text{kg/m}^3$; sound speed in air $c = 343.5\,\text{m/s}$; tension $T = 50\,\text{N}$; membrane mass density $\rho_m = 0.17\,\text{kg/m}^2$; frequency $f = 100\,\text{Hz}$; and spring constants $\bar{k}_1 = \bar{k}_2 = \bar{k}_3 = \bar{k}_4 = 1$.

Fig. 4.2 shows the real components of the dimensionless normal velocities $\phi^s_{1z}(x, y, z)$ and $\phi^s_{2z}(x, y, z)$ plotted against x and y at $z = -L$. It is evident that both components exhibit consistent behavior, as expected from the continuity condition of normal velocities at $z = -L$.

Similarly, Fig. 4.3 presents the imaginary components of the dimensionless normal velocities $\phi^s_{1z}(x, y, z)$ and $\phi^s_{2z}(x, y, z)$ against x and y at $z = -L$. Again, both components demonstrate matching behavior, in line with the continuity condition of normal velocities at $z = -L$.

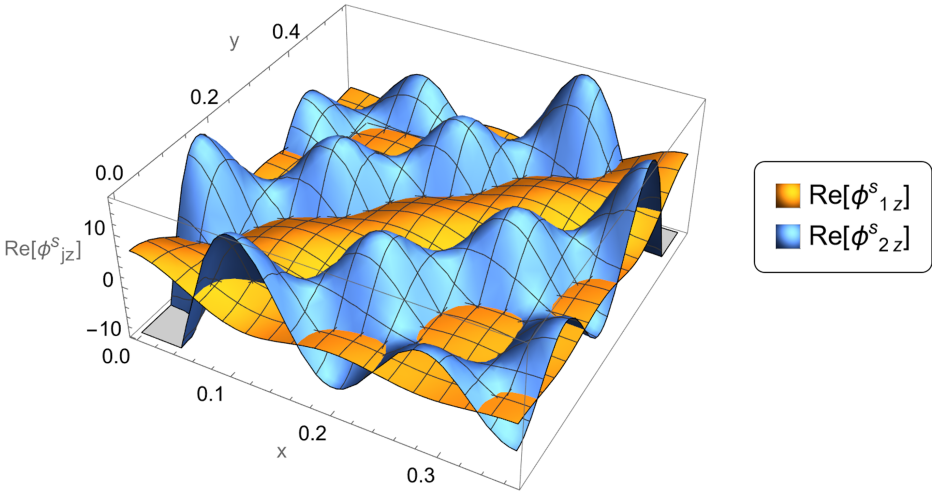

FIGURE 4.2: The real components of dimensionless normal velocities $\phi^s_{1z}(x, y, z)$ and $\phi^s_{2z}(x, y, z)$ against x and y at $z = -L$, where $\bar{a} = 0.2$m, $\bar{b} = 0.3$m, $\bar{L} = 0.1$m and N = 6 terms (Symmetric Case)

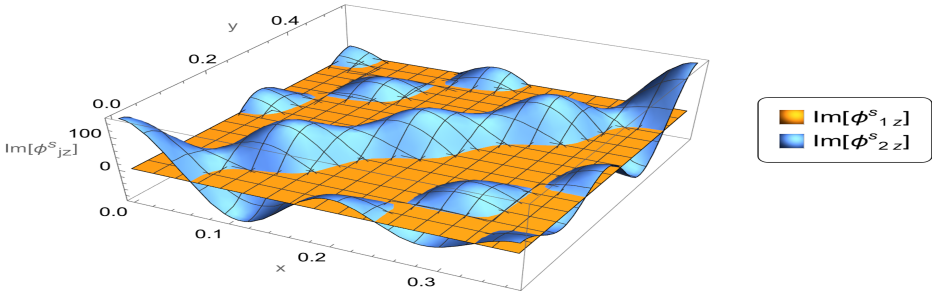

FIGURE 4.3: The imaginary components of dimensionless normal velocities $\phi^s_{1z}(x, y, z)$ and $\phi^s_{2z}(x, y, z)$ against x and y at $z = 0$, where $\bar{a} = 0.2$m, $\bar{b} = 0.3$m, $\bar{L} = 0.1$m and N = 6 terms (Symmetric Case)

To examine the behavior of the wave at the rigid wall, the real part of the symmetric normal velocity is presented in Fig. 4.4. It is observed that the velocity becomes zero at the rigid wall, which is consistent with the boundary condition imposed by the wall. This result aligns with the physical expectation that a rigid boundary should prevent any normal motion of the wave at the wall.

On the other hand, the symmetric pressure field does not vanish at the wall, as shown in Fig. 4.5. The pressure field exhibits a clear reflection at the wall, indicating that the incident wave is reflected back upon encountering the rigid surface.

This reflects that the pressure field exerts a force on the membrane situated at the interfaces, causing it to vibrate. The interaction between the incident and reflected pressure fields at the wall plays a crucial role in the overall wave dynamics within the cavity, influencing both the pressure distribution and the membrane's vibrational response.

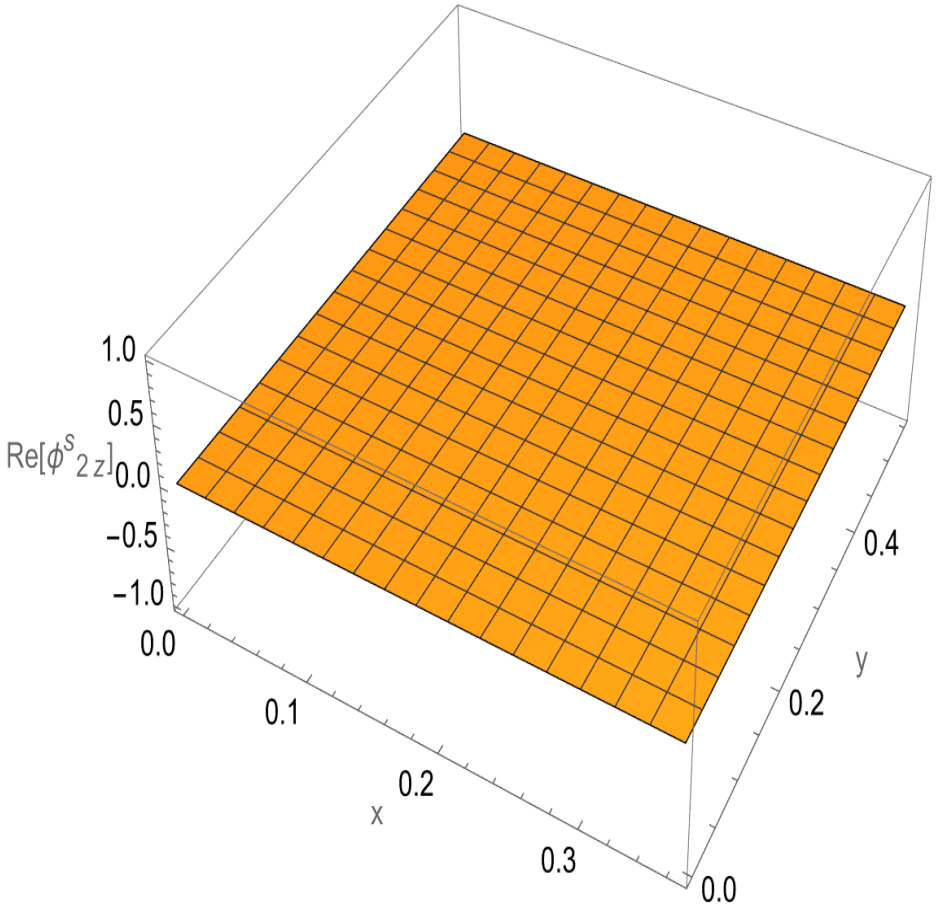

FIGURE 4.4: The real component of dimensionless normal velocity $\phi^s_{2z}(x, y, z)$ against x and y at $z = -L$, where $\bar{a} = 0.2$m, $\bar{b} = 0.3$m, $\bar{L} = 0.1$m and N = 6 terms (Symmetric Case)

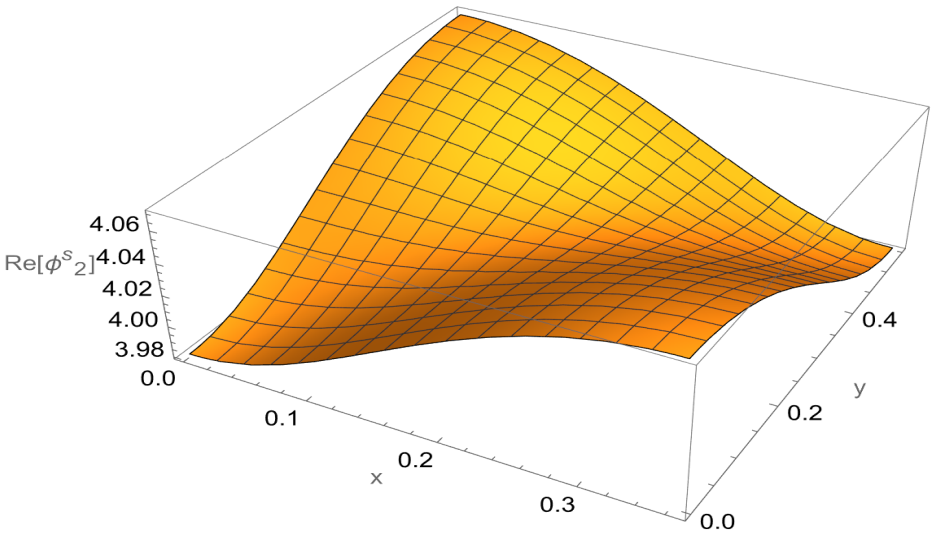

FIGURE 4.5: The real component of dimensionless pressure $\phi_2^s(x, y, z)$ against x and y at $z = 0$, where $\bar{a} = 0.2$m, $\bar{b} = 0.3$m, $\bar{L} = 0.1$m and N = 6 terms (Symmetric Case)

The imaginary part of the symmetric normal velocity at the rigid wall is shown in Fig. 4.6. It can be seen that the velocity is zero at the wall, which is consistent with the boundary condition for a rigid surface. This confirms that the wall effectively restricts any normal motion of the wave. In contrast, the symmetric pressure field at the wall is not zero, as illustrated in Fig. 4.7. The reflected pressure field at the wall is clearly visible, indicating that the incident wave is reflected upon striking the rigid surface. This reflected pressure creates a force on the membrane positioned at the interfaces, leading to membrane vibrations. The interaction between the incident and reflected pressure fields significantly influences the pressure distribution and the dynamic response of the membrane.

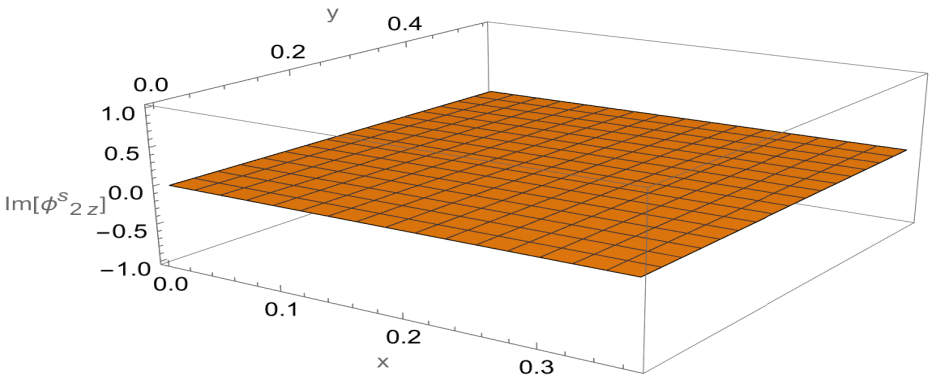

FIGURE 4.6: The imaginary component of dimensionless normal velocity $\phi_{2_z}^s(x, y, z)$ against x and y at $z = -L$, where $\bar{a} = 0.2$m, $\bar{b} = 0.3$m, $\bar{L} = 0.1$m and N = 6 terms (Symmetric Case)

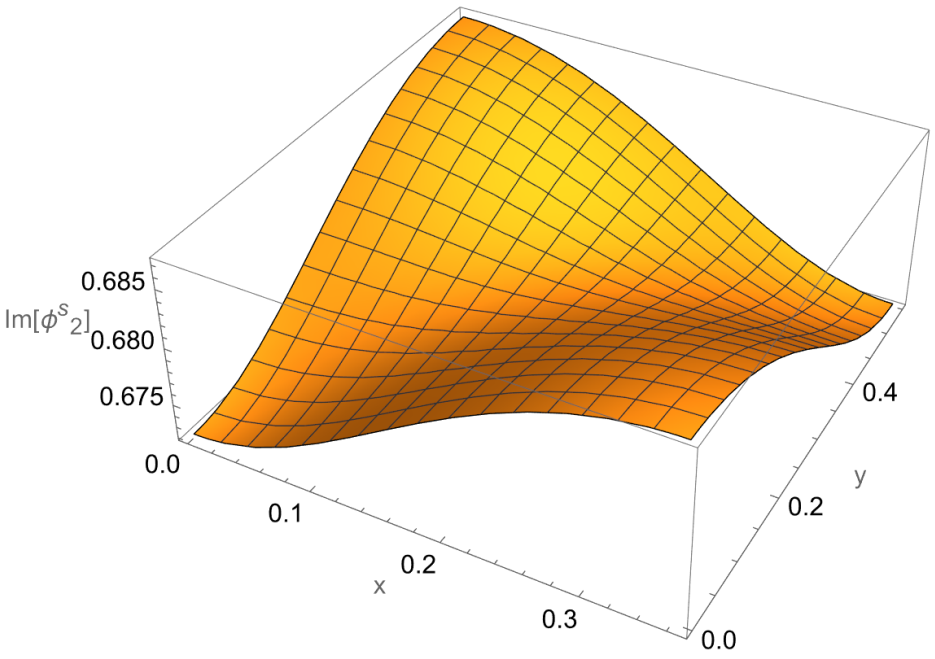

FIGURE 4.7: The imaginary component of dimensionless pressure $\phi_2^s(x, y, z)$ against x and y at $z = 0$, where $\bar{a} = 0.2$m, $\bar{b} = 0.3$m, $\bar{L} = 0.1$m and N = 6 terms (Symmetric Case)

4.4 Scattering of Acoustic Wave from a Rectangular Membrane Backed by Soft wall

Consider a duct mode incident on a membrane sheet of area "ab" located at $z = -\ell$. There is a soft wall located at $z = 0$ and incident mode is coming from $z < -\ell$. The geometry of waveguide is as shown in Fig. 4.8.

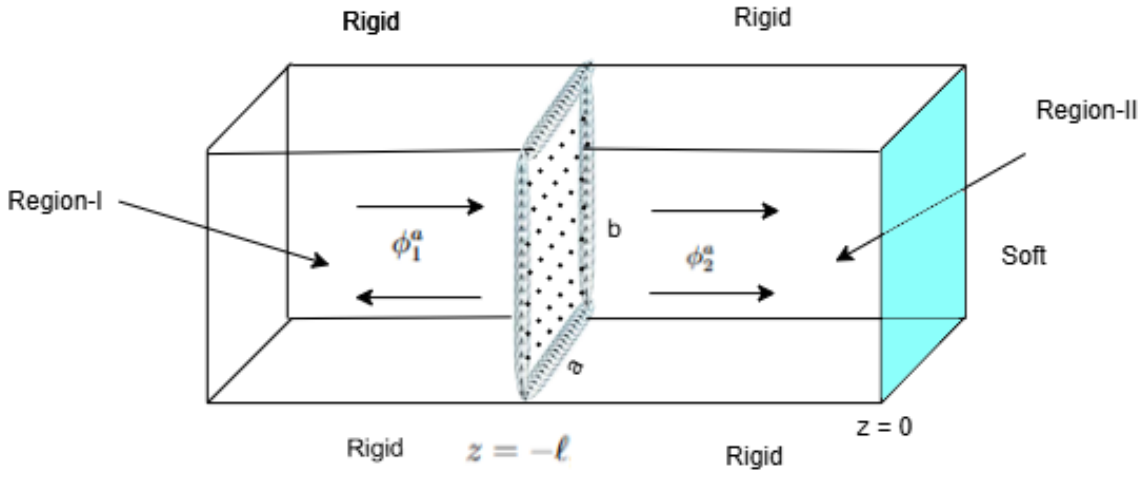

FIGURE 4.8: The physical configuration of waveguide

The fluid potentials in region-I and region-II can be expressed as:

$$\phi^a(x,y) = \begin{cases} \phi_1^a(x,y) & z < -\ell, \\ \phi_2^a(x,y) & z > -\ell, \end{cases} \tag{4.56}$$

where superscript "a" represent antisymmetric regions. These satisfies the Helmholtz's equation along with rigid boundary conditions. These governing equations are:

$$\{\nabla^2 + k^2\}\phi^a = 0, \tag{4.57}$$

$$\frac{\partial \phi_1^a}{\partial x} = 0, \qquad x = 0, \qquad x = a, \qquad 0 < y < b, \tag{4.58}$$

$$\frac{\partial \phi_2^a}{\partial y} = 0, \qquad x = 0, \qquad x = b, \qquad 0 < x < a. \tag{4.59}$$

The fluid potentials can be written in eigenfunction expansion form as:

$$\phi_1^a(x,y,z) = \sum_{m=0}^{\infty}\sum_{n=0}^{\infty}\left(A_{mn}^a e^{i\eta_{mn}(z+l)} + B_{mn}^a e^{-i\eta_{mn}(z+l)}\right)\psi_{mn}(x,y), \tag{4.60}$$

and

$$\phi_2^a(x,y,z) = \sum_{m=0}^{\infty}\sum_{n=0}^{\infty}\left(C_{mn}^a e^{i\eta_{mn}z} + D_{mn}^a e^{-i\eta_{mn}z}\right)\psi_{mn}(x,y). \tag{4.61}$$

But as at $z = 0$, there exist a soft wall, that gives

$$\phi_2^a(x,y) = 0, \qquad z = 0. \tag{4.62}$$

By using (4.61) into (4.62), we may get

$$\sum_{m=0}^{\infty}\sum_{n=0}^{\infty}(C_{mn}^a + D_{mn}^a)\eta_{mn}\psi_{mn}(x,y) = 0, \tag{4.63}$$

simplification leads to

$$D_{mn}^a = -C_{mn}^a. \tag{4.64}$$

By using the value of D_{mn}^a, from (4.64) into (4.61), we find

$$\phi_2^a(x,y,z) = \sum_{m=0}^{\infty}\sum_{n=0}^{\infty} 2iC_{mn}^a \sin(\eta_{mn}z)\psi_{mn}(x,y). \tag{4.65}$$

Here the coefficient C^a_{mn} and B^a_{mn} are unknowns once A^a_{mn} is provided to the system for excitation of duct modes. As there lies a membrane at $z = -\ell$, we consider its dynamics using Galerkin method to find the unknown amplitudes.

4.5 Galerkin Formulation for Membrane Dynamics

The dynamical response of membrane at interface $z = -\ell$, can be given as:

$$\nabla^2 u^a(x,y) + \mu^2 u^a(x,y) = \alpha(\phi^a_2 - \phi^a_1), \tag{4.66}$$

subject to the boundary conditions:

$$\frac{\partial u^a(x,y)}{\partial x} - k_1 u^a(x,y) = 0, \qquad x = 0, \tag{4.67}$$

$$\frac{\partial u^a(x,y)}{\partial x} + k_2 u^a(x,y) = 0, \qquad x = a, \tag{4.68}$$

$$\frac{\partial u^a(x,y)}{\partial y} - k_3 u^a(x,y) = 0, \qquad y = 0, \tag{4.69}$$

$$\frac{\partial u^a(x,y)}{\partial y} + k_4 u^a(x,y) = 0, \qquad y = b. \tag{4.70}$$

Here, we assume the solution in generalized Fourier series form as:

$$u^a(x,y) = \sum_{p=0}^{\infty}\sum_{q=0}^{\infty} J^a_{pq}\chi^a_{pq}(x,y), \tag{4.71}$$

where $\chi^a_{pq}(x,y)$ satisfies the eigenvalue problem associated with (4.66)

$$\nabla^2 \chi_{pq} + \lambda^2_{pq}\chi^a_{pq} = 0, \tag{4.72}$$

with subject to boundary conditions:

$$\frac{\partial \chi_{pq}(x,y)}{\partial x} - k_1 \chi_{pq}(x,y) = 0, \qquad x = 0, \tag{4.73}$$

$$\frac{\partial \chi_{pq}(x,y)}{\partial x} + k_2 \chi_{pq}(x,y) = 0, \qquad x = a, \tag{4.74}$$

$$\frac{\partial \chi_{pq}(x,y)}{\partial y} - k_3 \chi_{pq}(x,y) = 0, \qquad y = 0, \tag{4.75}$$

$$\frac{\partial \chi_{pq}(x,y)}{\partial y} + k_4 \chi_{pq}(x,y) = 0, \qquad y = b. \tag{4.76}$$

Note that J^a_{pq} is unknown that will be found through (4.66). However, to determine χ^a_{pq}, we solve eigenvalue problem given by (4.72) to (4.76). For sake of generality we assume

$$\chi^a_{pq} = X_p Y_q. \tag{4.77}$$

By using (4.77) into (4.72), we may get

$$\frac{X_p{}''}{X_p} = -\frac{Y_q{}''}{Y_q} - \lambda^2_{pq} = -\gamma_p^2, \tag{4.78}$$

whereas, for $X_p(x)$, the ordinary differential equation is

$$X_p{}''(x) + \gamma_p^2 X_p(x) = 0. \tag{4.79}$$

The solution of (4.79), is

$$X_p = c_{21}\cos(\gamma_p x) + c_{22}\sin(\gamma_p x), \tag{4.80}$$

where c_{21} and c_{22} are arbitrary constants. By using (4.73) into (4.80), we may get

$$X_p = c_{22}\left(\frac{\gamma_p}{k_1}\cos(\gamma_p x) + \sin(\gamma_p x)\right). \tag{4.81}$$

On using (4.74) into (4.81), we obtain

$$c_{22}\left(\left(1+\frac{k_2}{k_1}\right)\gamma_p\cos(\gamma_p a) + \left(k_2 - \frac{\gamma_p^2}{k_1}\right)\sin(\gamma_p a)\right) = 0. \tag{4.82}$$

For nontrivial solution, $c_{22} \neq 0$, then (4.82) can be rewritten as

$$\left(\left(1+\frac{k_2}{k_1}\right)\gamma_p\cos(\gamma_p a) + \left(k_2 - \frac{\gamma_p^2}{k_1}\right)\sin(\gamma_p a)\right) = 0. \tag{4.83}$$

Here, the roots of equation (4.83), denoted as γ_p, will be obtained using numerical method like Newton - Raphson or Secant method. Hence

$$X_p = \frac{\gamma_p}{k_1}\cos(\gamma_p x) + \sin(\gamma_p x). \tag{4.84}$$

Here, X_p are orthogonal, satisfying orthogonality relation that is

$$\int_0^a X_p X_l dx = \delta_{pl} E_l, \tag{4.85}$$

where

$$E_l = \int_0^a X_l^2 dx, \tag{4.86}$$

whereas, for $Y_q(y)$, the ordinary differential equation is

$$Y_q{}'' + \gamma_q^2 Y_q = 0, \quad \text{with} \quad \gamma_q = \sqrt{\lambda_{pq}^2 - \gamma_p^2}. \tag{4.87}$$

The solution of equation (4.87), is

$$Y_q = c_{23}\cos(\gamma_q y) + c_{24}\sin(\gamma_q y), \tag{4.88}$$

where c_{23} and c_{24} are arbitrary constants. By using (4.75) into (4.88), we obtain

$$Y_q = c_{24}\left(\frac{\gamma_q}{k_3}\cos(\gamma_q y) + \sin(\gamma_q y)\right). \tag{4.89}$$

On using (4.76) into (4.89), we obtain

$$c_{24}\left(\left(1 + \frac{k_4}{k_3}\right)\gamma_q \cos(\gamma_q b) + \left(k_4 - \frac{\gamma_q^2}{k_3}\right)\sin(\gamma_q b)\right) = 0. \tag{4.90}$$

For nontrivial solution, $c_{24} \neq 0$, then (4.90) can be written as:

$$\left(\left(1+\frac{k_4}{k_3}\right)\gamma_q\cos(\gamma_q b)+\left(k_4-\frac{\gamma_q^2}{k_3}\right)\sin(\gamma_q b)\right)=0. \tag{4.91}$$

Here, the roots of equation (4.91), denoted as γ_q, will be obtained using numerical method like Newton - Raphson or Secant method. Hence

$$Y_q=\frac{\gamma_q}{k_2}\cos(\gamma_q y)+\sin(\gamma_q y). \tag{4.92}$$

Here, Y_q are orthogonal, satisfying orthogonality relation that is

$$\int_0^a Y_q Y_m dy=\delta_{qm}F_m, \tag{4.93}$$

where

$$F_m=\int_0^b Y_m^2 dy. \tag{4.94}$$

In order to show orthogonality we reconsider (4.77), which is

$$\chi_{pq}^a=X_pY_q. \tag{4.95}$$

On multiplying by χ_{lm}^a and integrating over $0<x<a$ and $0<y<b$, we may get

$$\int_0^a\int_0^b \chi_{pq}^a\chi_{lm}^a dxdy=\Gamma_{lm}\delta_{pl}\delta_{qm}. \tag{4.96}$$

By using orthogonality relation (4.96), and simplifying, we get

$$\Gamma_{lm}=E_lF_m. \tag{4.97}$$

The value of χ_{pq}^a, is

$$\chi_{pq}^a=\left(\frac{\gamma_p}{k_1}\cos(\gamma_p x)+\sin(\gamma_p x)\right)\left(\frac{\gamma_q}{k_2}\cos(\gamma_q y)+\sin(\gamma_q y)\right). \tag{4.98}$$

On multiplying we get the following form

$$\begin{aligned}\chi_{pq}^a=&\frac{\gamma_p\gamma_q}{k_1k_2}\cos(\gamma_p x)\cos(\gamma_q y)+\frac{\gamma_p}{k_1}\cos(\gamma_p x)\sin(\gamma_q y)+\frac{\gamma_q}{k_2}\cos(\gamma_q y)\sin(\gamma_p x)\\&+\sin(\gamma_p x)\sin(\gamma_q y).\end{aligned} \tag{4.99}$$

By using (4.60),(4.65) and (4.71) into (3.66), we may get

$$\sum_{p=0}^{\infty}\sum_{q=0}^{\infty} J^a_{pq}(\mu^2-\lambda^2_{pq})\chi^a_{pq} = \alpha\sum_{m=0}^{\infty}\sum_{n=0}^{\infty}(A^a_{mn}+B^a_{mn}-2iC^a_{mn}\sin(\eta_{mn}l))\psi_{mn}. \tag{4.100}$$

On multiplying with χ^a_{lm} and integrating over $0<x<a$ and $0<y<b$, we may get

$$J^a_{lm} = \frac{\alpha}{(\mu^2-\lambda^2_{lm})\Gamma_{lm}}\sum_{r=0}^{\infty}\sum_{n=0}^{\infty}(A^a_{rn}+B^a_{rn}+2iC^a_{rn}\sin(\eta_{rn}l))\Delta_{rnlm}. \tag{4.101}$$

By using orthogonality relation (4.101), and simplifying, we get

$$\Delta_{rnlm} = \int_0^a\int_0^b \chi_{lm}\psi_{rn}dxdy. \tag{4.102}$$

Accordingly, for region-I, at $z=-\ell$, we have

$$\frac{\partial\phi^a_1}{\partial z} = u^a(x,y). \tag{4.103}$$

By using (4.60) and (4.71) into (4.103), we may get

$$i\sum_{m=0}^{\infty}\sum_{n=0}^{\infty}(A^a_{mn}-B^a_{mn})\eta_{mn}\psi_{mn}(x,y) = \sum_{p=0}^{\infty}\sum_{q=0}^{\infty}J^a_{pq}\chi^a_{pq}. \tag{4.104}$$

Multiplying by ψ_{gj} with (4.104) and integrating over $0<x<a$ and $0<y<b$, we may get

$$A^a_{gj}-B^a_{gj} = \frac{1}{i\eta_{gj}\triangle_{gj}}\sum_{p=0}^{\infty}\sum_{q=0}^{\infty}J^a_{pq}\Delta_{gjpq}, \tag{4.105}$$

where

$$\Delta_{gjpq} = \int_0^a\int_0^b \psi_{gj}\chi_{pq}. \tag{4.106}$$

Similarly, for region-II, at $z=-\ell$, we have

$$\frac{\partial \phi_2^a}{\partial z} = u^a(x, y). \tag{4.107}$$

By using (4.65) and (4.71) into (4.107), we may get

$$\sum_{m=0}^{\infty}\sum_{n=0}^{\infty} 2iC_{mn}^a \eta_{mn} \cos(\eta_{mn} l)\psi_{mn}(x, y) = \sum_{p=0}^{\infty}\sum_{q=0}^{\infty} J_{pq}^a \chi_{pq}. \tag{4.108}$$

By using orthogonality relation, after some mathematical rearrangements, it is found that

$$C_{gj}^a = \frac{1}{2i\cos(\eta_{gj} l)\eta_{gj} \triangle_{gj}} \sum_{p=0}^{\infty}\sum_{q=0}^{\infty} J_{pq}^a \bigwedge_{gjpq}, \tag{4.109}$$

where

$$\bigwedge_{gjpq} = \int_0^a \int_0^b \psi_{gj}\chi_{pq} dxdy. \tag{4.110}$$

4.6 Numerical Results for Soft Wall

The problem of a soft cavity with an anti-symmetric configuration is addressed numerically by truncating the series up to N terms.

The numerical calculations are performed using the software *MATHEMATICA*, with the following set of parameters: membrane dimensions $\bar{a} = 0.2\,\text{m}$, $\bar{b} = 0.3\,\text{m}$; cavity length $\bar{L} = 0.1\,\text{m}$; air density $\rho = 1.2\,\text{kg/m}^3$; speed of sound in air $c = 343.5\,\text{m/s}$; membrane tension $T = 50\,\text{N}$; membrane mass density $\rho_m = 0.17\,\text{kg/m}^2$; frequency $f = 100\,\text{Hz}$; and spring constants $\bar{k}_1 = \bar{k}_2 = \bar{k}_3 = \bar{k}_4 = 1$.

Fig. 4.9 illustrates the real components of the dimensionless normal velocities $\phi_{1z}^a(x, y, z)$ and $\phi_{2z}^a(x, y, z)$ as functions of x and y at $z = -L$ for the soft-backed cavity. It can be observed that both components exhibit similar behavior, which is consistent with the continuity condition of normal velocities at $z = -L$.

Similarly, Fig. 4.10 shows the imaginary components of the dimensionless normal velocities $\phi^a_{1z}(x, y, z)$ and $\phi^a_{2z}(x, y, z)$ against x and y at $z = -L$ for the soft-backed cavity. Once again, both components display consistent behavior, aligning with the continuity condition of normal velocities at $z = -L$.

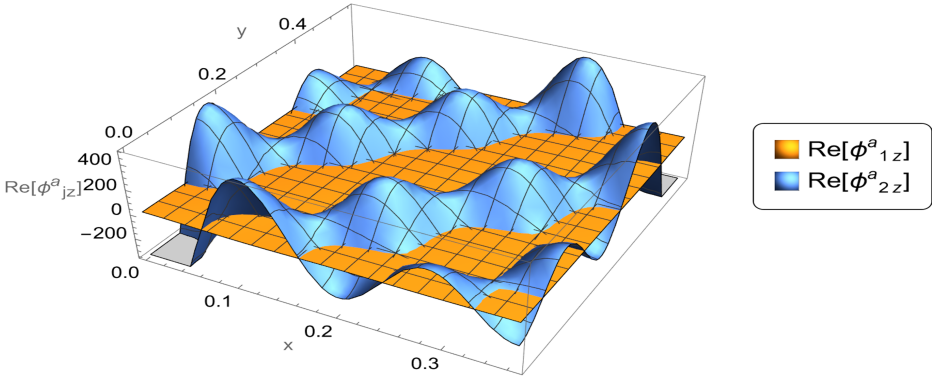

FIGURE 4.9: The real components of dimensionless normal velocities $\phi^a_{1z}(x, y, z)$ and $\phi^a_{2z}(x, y, z)$ against x and y at $z = -L$, where $\bar{a} = 0.2$m, $\bar{b} = 0.3$m, $\bar{L} = 0.1$m and N = 6 terms (Anti-symmetric Case)

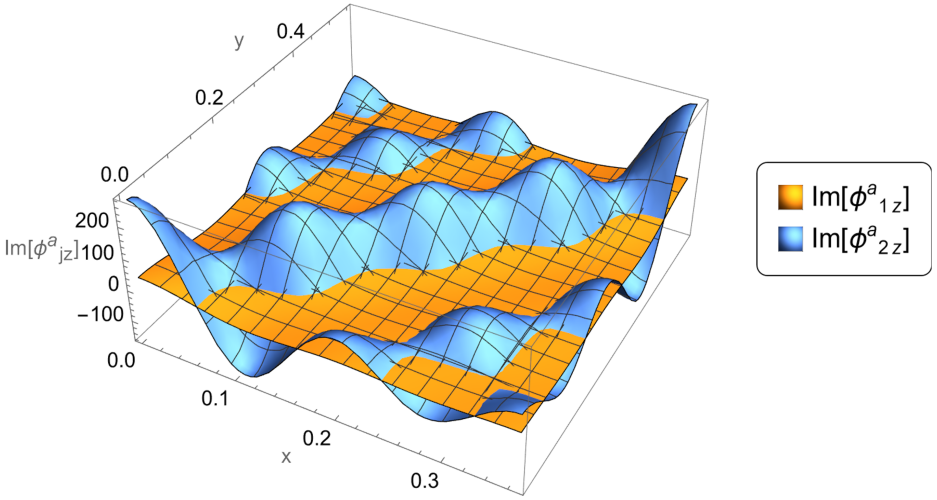

FIGURE 4.10: The imaginary components of dimensionless normal velocities $\phi^a_{1z}(x, y, z)$ and $\phi^a_{2z}(x, y, z)$ against x and y at $z = 0$, where $\bar{a} = 0.2$m, $\bar{b} = 0.3$m, $\bar{L} = 0.1$m and N = 6 terms (Anti-symmetric Case)

To investigate the behavior of the wave at the soft wall, the real part of the anti-symmetric normal velocity is shown in Fig. 4.11. It is evident that the normal

velocity is not zero at the soft wall, which is consistent with the boundary condition imposed by a soft surface. This result aligns with the physical expectation that a soft boundary allows normal motion of the wave at the wall, unlike a rigid boundary that would restrict it. The nonzero normal velocity at the soft wall reflects the fact that the wall can accommodate the wave's displacement, influencing the energy transfer and wave propagation within the cavity.

In contrast, the anti-symmetric pressure field becomes zero at the soft wall, as shown in Fig. 4.12. This implies that no net force is exerted by the pressure field at the wall, consistent with the soft boundary condition.

The vanishing pressure field at the wall signifies that the soft surface does not resist the wave's pressure, allowing the wave to adjust freely at the boundary. The presence of a soft wall introduces greater flexibility into the system, affecting the wave reflection and transmission characteristics and modifying the overall pressure and velocity distribution within the cavity.

This makes the soft-backed cavity more responsive to incident waves, which can have practical significance in acoustic absorption and vibration control applications.

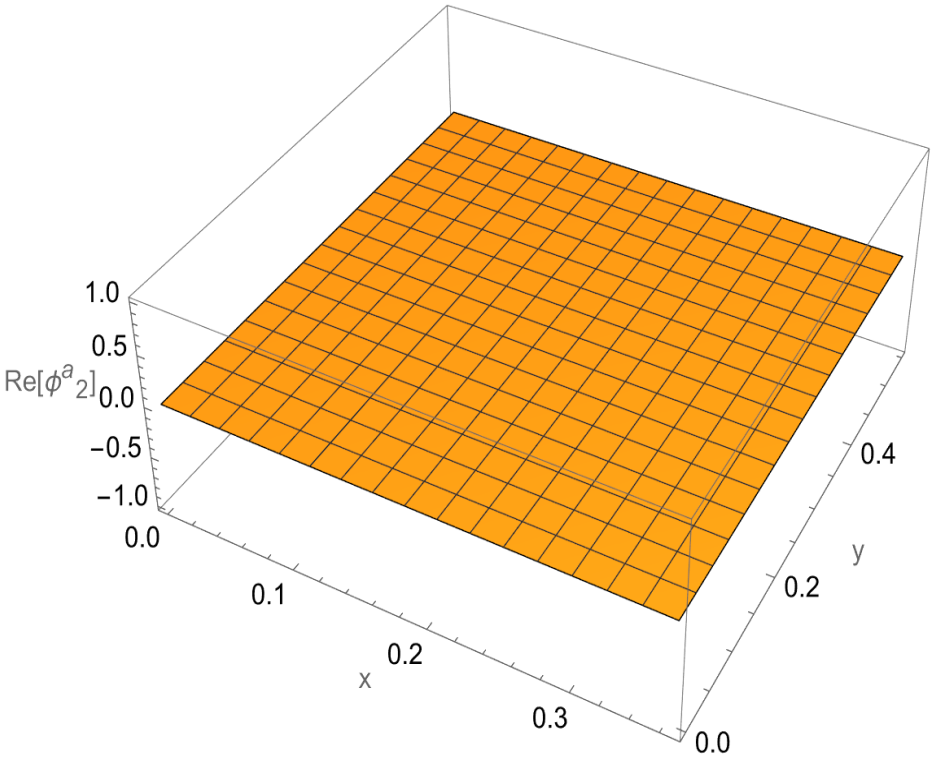

FIGURE 4.11: The real component of pressure $\phi_2^a(x, y, z)$ against x and y at $z = -L$, where $\bar{a} = 0.2$m, $\bar{b} = 0.3$m, $\bar{L} = 0.1$m and N = 6 terms (Anti-symmetric Case)

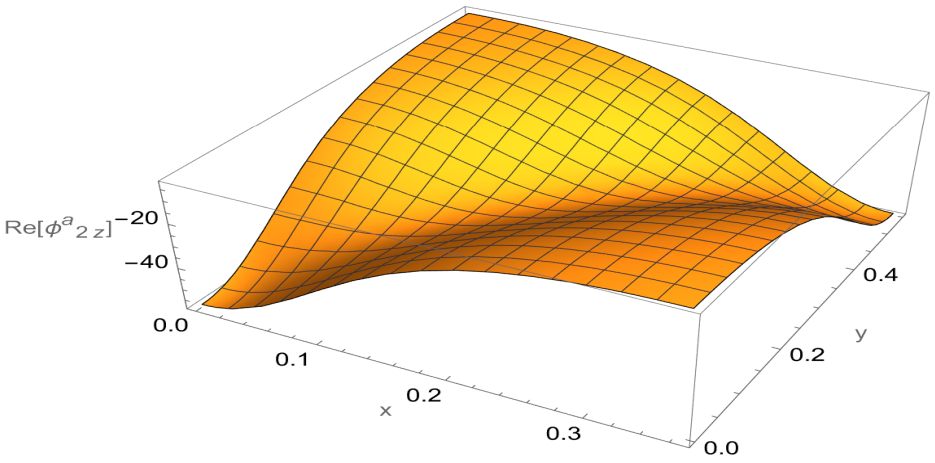

FIGURE 4.12: The real component of dimensionless normal velocity $\phi^a_{2z}(x, y, z)$ against x and y at $z = 0$, where $\bar{a} = 0.2$m, $\bar{b} = 0.3$m, $\bar{L} = 0.1$m and N = 6 terms (Anti-symmetric Case)

The imaginary part of the anti-symmetric normal velocity at the soft wall is shown in Fig. 4.13. It can be seen that the velocity is not zero at the wall, which is consistent with the boundary condition for a soft surface. This confirms that the soft wall allows normal motion of the wave, unlike a rigid wall that would restrict it.

In contrast, the anti-symmetric pressure field at the wall is zero, as illustrated in Fig. 4.14. This implies that no net force is exerted by the pressure field at the soft wall, which aligns with the boundary condition for a soft surface. The absence of a reflected pressure field at the wall indicates that the wave is not reflected in terms of pressure, allowing the membrane at the interfaces to adjust more freely. This behavior significantly affects the pressure distribution and the dynamic response of the membrane, influencing the overall wave propagation within the cavity.

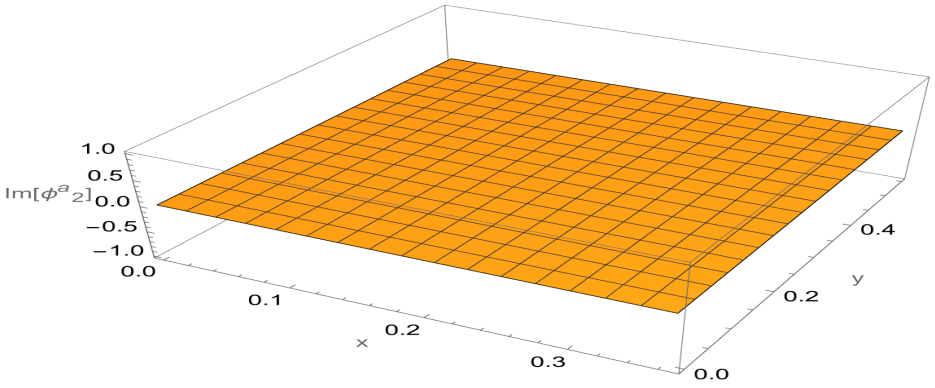

FIGURE 4.13: The imaginary component of dimensionless pressure $\phi^a_2(x, y, z)$ against x and y at $z = -L$, where $\bar{a} = 0.2$m, $\bar{b} = 0.3$m, $\bar{L} = 0.1$m and N = 6 terms (Anti-symmetric Case)

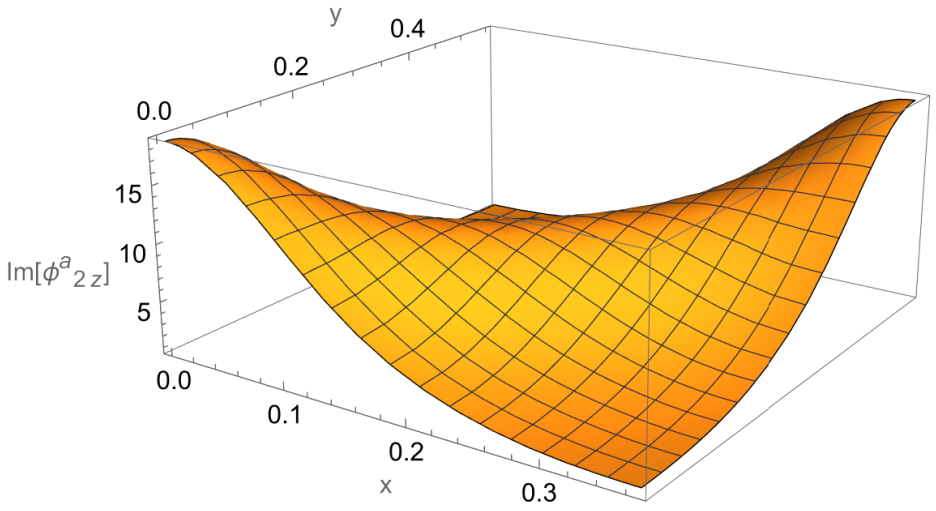

FIGURE 4.14: The imaginary component of dimensionless normal velocity $\phi^a_{2z}(x, y, z)$ against x and y at $z = 0$, where $\bar{a} = 0.2$m, $\bar{b} = 0.3$m, $\bar{L} = 0.1$m and N = 6 terms (Anti-symmetric Case)

Chapter 5

Conclusion

The present thesis is focused on the modelling of rectangular elastic membrane in waveguide and then finding the solution of governing boundary value problem by using Mode-Matching method. For sake of generality the edges of the membrane are assumed to contain spring like edge conditions. Acoustic radiation are made incident in normal direction to the membrane which after interaction with membrane are reflected and transmitted. Various modes in membrane can be excited to optimize the scattering characteristic of the waveguide. Three problems are solved in this thesis by assuming different types of boundary conditions along the membrane.

In Chapter 3, the vertical membrane is assumed in an infinite 3-dimensional waveguide. The acoustic response across the membrane is expressed by using the eigenfunction expansion forms. The membrane response is coupled with fluid and is found by applying the Galerkin's formulation. The displacement is projected on orthogonal basis and involve Fourier coefficient as unknowns. The matching conditions at interface are applied to convert the system into linear algebraic systems which was be truncated and solved by numerically. The membrane and acoustic modes are shown numerically for fixed setting of involved parameters.

In Chapter 4, two problems are discussed, first problem contains the elastic membrane in 3-dimensional duct backed by rigid cavity. The symmetric modes propagate in the duct which are found by applying the Mode-Matching method along with Galerkin formulation. In the second problem the membrane is assumed to backed by

soft wall condition. The anti-symmetric modes exist in the setting that calculated by used the Mode-Matching technique.

For the symmetric mode, it was observed that the normal velocity at the soft wall is zero, which is consistent with the boundary condition for a rigid surface. This confirms that a symmetric wave mode imposes a restriction on the normal motion of the wave at the wall, resulting in a reflected pressure field. The nonzero symmetric pressure field at the wall generates a force on the membrane positioned at the interfaces, causing it to vibrate. The interaction between the incident and reflected pressure fields significantly influences the pressure distribution and the dynamic response of the membrane, affecting the overall wave dynamics within the cavity. In contrast, for the anti-symmetric mode, the normal velocity at the soft wall was found to be nonzero, consistent with the boundary condition for a soft surface. This reflects the fact that a soft boundary allows normal motion of the wave at the wall, leading to increased flexibility and energy transfer within the cavity. However, the anti-symmetric pressure field at the soft wall was observed to be zero, indicating the absence of reflected pressure. This implies that the soft boundary does not resist the pressure field, allowing the wave to adjust freely at the boundary.

The study highlights the distinct behavior of symmetric and anti-symmetric modes in a soft-backed cavity. While symmetric modes result in reflected pressure fields and restricted normal velocity at the wall, anti-symmetric modes lead to nonzero normal velocity and zero pressure at the wall. These findings provide valuable insights into the influence of boundary conditions on wave dynamics within cavities and have important implications for the design and optimization of acoustic and structural systems involving soft-walled cavities.

Bibliography

[1] L. Cao and X. Wang. Optimization of acoustic membrane panel for sound absorption. *Journal of Sound and Vibration*, 330(11):2720–2734, 2011.

[2] C. Wang, L. Cai, M. Gao, L. Jin, L. Sun, X. Tang, G. Shi, X. Zheng, and C. Guo. Manufacturing of membrane acoustical metamaterials for low frequency noise reduction and control: a review. *Mechanics of Advanced Materials and Structures*, 31(25):7008–7023, 2024.

[3] C. J. Naify, C.-M. Chang, G. McKnight, and S. Nutt. Transmission loss and dynamic response of membrane-type locally resonant acoustic metamaterials. *Journal of Applied Physics*, 108(11), 2010.

[4] M. Boccaccio, K. Myronidis, M. Thielke, M. Meo, and F. Pinto. A multifunctional ultra-thin acoustic membrane with self-healing properties for adaptive low-frequency noise control. *Scientific Reports*, 12(1):17790, 2022.

[5] D.-Y. Maa. Potential of microperforated panel absorber. *The Journal of the Acoustical Society of America*, 104(5):2861–2866, 1998.

[6] X.-L. Gai, T. Xing, X.-H. Li, B. Zhang, and W.-J. Wang. Sound absorption of microperforated panel mounted with helmholtz resonators. *Applied Acoustics*, 114:260–265, 2016.

[7] C. Li, B. Cazzolato, and A. Zander. Acoustic impedance of micro perforated membranes: Velocity continuity condition at the perforation boundary. *The Journal of the Acoustical Society of America*, 139(1):93–103, 2016.

[8] Y. Y. Lee, E. W. M. Lee, and C. F. Ng. Sound absorption of a finite flexible micro-perforated panel backed by an air cavity. *Journal of Sound and Vibration*, 287:227–243, 2005.

[9] W. Guo and H. Min. A compound micro-perforated panel sound absorber with partitioned cavities of different depths. *Energy Procedia*, 78:1617–1622, 2015.

[10] J. Kang and H. V. Fuchs. Predicting the absorption of open weave textiles and microperforated membranes backed by an air space. *Journal of Sound and Vibration*, 220:905–920, 1999.

[11] J. Liu and W. Chen. Effect of restrain edge on sound radiation of membrane panels with different materials. *Journal of Sound and Vibration*, 473:115242, 2020. doi: 10.1016/j.jsv.2020.115242.

[12] G. Wang, Y. Zhang, Z. Sheng, Z. Zhu, G. Li, and J. Ni. Analysis of the sound absorption characteristics of the curved microperforated panel with elastically restrained edges. *Thin-Walled Structures*, 182:110147, 2023.

[13] J. Liu and W. Chen. Effect of restrain edge on sound transmission loss of membrane panels. *Journal of Sound and Vibration*, 443:247–258, 2019.

[14] M. Afzal and M. Safdar. Mode-matching technique for analyzing scattering in elastic shell chambers: Applications in trifurcated waveguide systems. *Communication in Nonlinear Science and Numerical Simulation*, 130:107723, 2023. doi: 10.1016/j.cnsns.2023.107723.

[15] H. Bilal, M. U. Khan, and M. Afzal. Silencing performance of the wave-bearing cavity with porous media. *Journal of Vibration and Control*, 2023. doi: 10.1177/1077546323120938. URL https://doi.org/10.1177/1077546323120938.

[16] M. Afzal, M. O. Alkinidri, M. Safdar, and H. Bilal. On the scattering of cylindrical elastic shell having trifurcation and structural variations at interfaces. *Chaos, Solitons Fractals*, 175:114033, 2023. doi: 10.1016/j.chaos.2023.114033.

[17] M. Afzal, H. Bilal, N. Ahmed, and A. Wahab. Acoustic scattering from a wave-bearing cavity with flexible inlet and outlet. *Mathematical Methods in the Applied*

Sciences, 2023. doi: 10.1002/mma.9633. URL https://doi.org/10.1002/mma.9633.

[18] M. Safdar, N. Ahmed, M. Afzal, and A. Wahab. Acoustic scattering in lined panel cavities with membrane interfaces. *Journal of the Acoustical Society of America*, 154:1138–1151, 2023. doi: 10.1121/10.1002/mma.9633.

[19] M. Afzal, N. Akhtar, M. O. Alkinidri, and M. Shutaywi. A mode-matching tailored-galerkin approach for higher order interface conditions and geometric variations. *Mathematics*, 11(3):755, 2023. doi: 10.3390/math11030755.

[20] M. Afzal and H. Bilal. Silencing performance analysis of a membrane cavity with different edge conditions. *Journal of Vibration and Control*, 2022. doi: 10.1177/1077546322111870. URL https://doi.org/10.1177/1077546322111870.

[21] H. Bilal and M. Afzal. Reflection and transmission of acoustic waves through the bridging membrane junctions. *Waves in Random and Complex Media*, 2022. doi: 10.1080/17455030.2022.2051771. URL https://doi.org/10.1080/17455030.2022.2051771.

[22] Bilal and M. Afzal. On the extension of the mode-matching procedure for modeling a wave-bearing cavity. *Mathematics and Mechanics of Solids*, 27(2):348–367, 2022. doi: 10.1177/10812865211054100.

[23] M. Afzal, J. U. Satti, R. Nawaz, and A. Wahab. Scattering analysis of a partitioned membrane-bounded cavity with material contrast. *Journal of the Acoustical Society of America*, 151(1):31–44, 2022. doi: 10.1121/1.5123416.

[24] T. Nawaz, M. Afzal, and A. Wahab. Scattering analysis of a flexible trifurcated lined waveguide structure with step-discontinuities. *Physica Scripta*, 96 (11):115004, 2021. doi: 10.1088/1402-4896/ac0b34.

[25] M. Afzal, S. Shafique, and A. Wahab. Analysis of traveling waveform of flexible waveguides containing absorbent material along flanged junctions. *Communication in Nonlinear Science and Numerical Simulation*, 97:105737, 2021. doi: 10.1016/j.cnsns.2020.105737.

[26] M. Afzal and J. U. Satti. The traveling wave formulation of a splitting chamber containing reactive components. *Archive of Applied Mechanics*, 91:1959–1980, 2021. doi: 10.1007/s00419-020-01822-4.

[27] M. Afzal, T. Nawaz, and R. Nawaz. Scattering characteristics of planar trifurcated waveguide structure containing multiple discontinuities. *Waves in Random and Complex Media*, 2020. doi: 10.1080/17455030.2020.1864062.

[28] S. Shafique, M. Afzal, and R. Nawaz. On the attenuation of fluid–structure coupled modes in a nonplanar waveguide. *Mathematics and Mechanics of Solids*, 25(10):1831–1850, 2020. doi: 10.1177/1081286520929047.

[29] M. Afzal and S. Shafique. Attenuation analysis of flexural modes with absorbent lined flanges and different edge conditions. *Journal of the Acoustical Society of America*, 148(1):85–99, 2020. doi: 10.1121/10.0001534.

[30] M. Afzal, J. U. Satti, and R. Nawaz. Scattering characteristics of nonplanar trifurcated waveguides. *Meccanica*, 55:977–988, 2020. doi: 10.1007/s11012-019-01115-4.

[31] J. U. Satti, M. Afzal, and R. Nawaz. Scattering analysis of a partitioned wave-bearing cavity containing different material properties. *Physica Scripta*, 94: 115223, 2019. doi: 10.1088/1402-4896/ab1c94.

[32] T. Nawaz, M. Afzal, and R. Nawaz. The scattering analysis of trifurcated waveguide involving structural discontinuities. *Advances in Mechanical Engineering*, 11(7):1–10, 2019. doi: 10.1177/1687814019856078.

[33] H. Bilal and M. Afzal. Acoustic wave scattering from a wave-bearing cavity in a rectangular waveguide. *Journal of the Acoustical Society of America*, 144:1681, 2018. doi: 10.1121/1.5055302.

[34] A. Ullah, R. Nawaz, and M. Afzal. Fluid-structure coupled wave scattering in a flexible duct at the junction of planar discontinuities. *Advances in Mechanical Engineering*, 9(7):1–11, 2017. doi: 10.1177/1687814017711344.

[35] J. B. Lawrie and M. Afzal. Acoustic scattering in a waveguide with a height discontinuity bridged by a membrane: a tailored galerkin approach. *Journal of Engineering Mathematics*, 105(1):99–115, 2017. doi: 10.1007/s10665-017-9905-1.

[36] S. Shafique, M. Afzal, and R. Nawaz. On mode matching analysis of fluid-structure coupled wave scattering between two flexible waveguides. *Canadian Journal of Physics*, 95(6):581–589, 2017. doi: 10.1139/cjp-2016-0687.

[37] M. Afzal, R. Nawaz, and A. Ullah. Attenuation of dissipative device involving coupled wave scattering. *Applied Mathematics and Computation*, 290(1):154–163, 2016. doi: 10.1016/j.amc.2016.06.016.

[38] R. Nawaz, M. Afzal, and M. Ayub. Acoustic propagation in two-dimensional waveguide for membrane bounded ducts. *Communications in Nonlinear Science and Numerical Simulation*, 20(2):421–433, 2015. doi: 10.1016/j.cnsns.2014.05.020.

[39] M. Afzal, N. Ahmed, M. Safdar, and M. Umar. On the modeling of sound sources in waveguides with structural variations and sound-absorbent materials. *Communication in Nonlinear Science and Numerical Simulation*, 145:108714, 2025.

[40] H. Bilal and M. Afzal. Application of the matrix element method: A mode-matching approach for wave-bearing cavities in complex media. *Chaos, Solitons Fractals*, 189:115589, 2024.

[41] S. Rizvi and M. Afzal. Electromagnetic wave scattering in plasma beam-driven waveguides under strong magnetic fields. *Communications in Theoretical Physics*, 76:115502, 2024.

[42] M. Afzal and T. Nawaz. Trifurcated lined ducts: A comprehensive study on noise reduction strategies. *PLoS ONE*, 19(7):e0306115, 2024. doi: 10.1371/journal.pone.0306115. URL https://doi.org/10.1371/journal.pone.0306115.

[43] M. Afzal, T. Aziz, and H. M. S. Bahaidarah. Dynamical behavior of fluid–structure interaction in ducts with rigid and flexible interfaces: Modeling and analysis. *Partial Differential Equations in Applied Mathematics*, 11:100789, 2024. doi: 10.1016/j.padiff.2024.100789. URL https://doi.org/10.1016/j.padiff.2024.100789.

[44] S. Shafique, M. A. Ahmad, and M. Afzal. Optimizing the noise control in a two-layer conduit. *Physica Scripta*, 99:065227, 2024. doi: 10.1088/1402-4896/ad451e.

[45] M. Afzal, M. Safdar, and H. N. Alahmadi. Analyzing the impact of flexible shells and sound absorbent lining on acoustic wave behavior in ducts. *Mathematical Methods in the Applied Science*, 2024. doi: 10.1002/mma.10133. URL https://doi.org/10.1002/mma.10133.

[46] S. Shafique, A. Ahmad, and M. Afzal. Optimizing the noise control in a two-layer conduit. *Physica Scripta*, 99(6):065227, 2024.

[47] S. Rizvi and M. Afzal. Cold plasma-induced effects on electromagnetic wave scattering in waveguides: a mode-matching analysis. *Communications in Theoretical Physics*, 76(3):035501, 2024.

[48] A. D. Alruwaili, M. Afzal, H. N. Alahmadi, and A. Wahab. Wave scattering in cylindrical waveguides: Analyzing flexible shells and liner conditions. *Alexandria Engineering Journal*, 91:610–619, 2024.

[49] A. D. Alruwaili, M. Afzal, M. Tanveer, and H. N. Alahmadi. Analyzing monopole sources modeling with structural variations and material contrast: An analytical perspective. *Chaos, Solitons Fractals*, 179(1):114434, 2024.

[50] R. Mittra. Analytical techniques in the theory of guided waves. *Macmillan Series in Electrical Science*, 1971.

[51] C. P. Kok and R. Mittra. Mode matching technique for solving electromagnetic problems. *Journal of Applied Physics*, 42(10):3941–3946, 1971.

[52] P. C. Waterman. Matrix formulation of electromagnetic scattering. *Proceedings of the IEEE*, 53(8):805–812, 1965.

[53] W. C. Chen and Y. Wang. Mode matching technique for acoustic wave propagation in complex geometries. *The Journal of the Acoustical Society of America*, 142(4):2511–2518, 2017.

[54] Q. Deng, T. Du, H. Gomaa, Y. Cheng, and C. An. Methods of manipulation of acoustic radiation using metamaterials with a focus on polymers: Design and mechanism insights. *Polymers*, 16(17):2405, 2024.

[55] E. Reissner. The effect of transverse shear deformation on the bending of elastic plates. *Journal of Applied Mechanics*, 12(2):69–77, 1945.

[56] J. O. Dow. A bonded plate model for thin plate vibrations. *Journal of Sound and Vibration*, 94(2):251–265, 1984.

[57] C. S. Huang. A new approach to the analysis of rectangular plates with free edges. *Journal of Sound and Vibration*, 278(3):551–566, 2004.